Marilies Piskernik, BSc

Synthesis and characterization of MOF-based Li ion conductors

MASTER'S THESIS

to achieve the university degree of

Diplom-Ingenieurin

Master's degree programme: Technical Chemistry

submitted to

Graz University of Technology

Supervisor

Univ.-Prof. Dr. rer. nat. Martin Wilkening
Institute of Chemistry and Technology of Materials

Dr. Ilie Hanzu
Institute of Chemistry and Technology of Materials

Graz, November 2015

AFFIDAVIT

I declare that I have authored this thesis independently, that I have not used other than the declared sources/resources, and that I have explicitly indicated all material which has been quoted either literally or by content from the sources used. The text document uploaded to TUGRAZonline is identical to the present master‘s thesis dissertation.

Date

Signature

Danksagung

An dieser Stelle möchte ich mich bei all jenen bedanken, die durch ihre fachliche und persönliche Unterstützung zum Gelingen dieser Diplomarbeit beigetragen haben.

Mein Dank gilt Herrn Prof. Dr. Wilkening für das Bereitstellen dieses interessanten Themas und der Betreuung. Ebenso danke ich Herrn Dr. Ilie Hanzu für die Bereitschaft, die Co-Betreuung zu übernehmen, ohne dessen Hilfe diese Arbeit nicht zustande gekommen wäre. Weiters möchte ich mich bei allen Mitarbeitern der Arbeitsgruppe und des ICTM bedanken, welche mich ebenso tatkräftig unterstützt haben.

Mein besonderer Dank gilt meiner Familie, insbesondere meinen Eltern, die mir mein Studium ermöglicht und mich in all meinen Entscheidungen unterstützt haben. Herzlich bedanken möchte ich mich auch bei meiner Schwester, die mich immer wieder ermutigte und damit einen wesentlichen Teil zur Diplomarbeit beigetragen hat. Schließlich danke ich meinen Freunden während der Studienzeit für sehr schöne Jahre in Graz.

Table of contents

1 Abstract

Two different types of metal organic frameworks (MOF), aluminium- and zirconium-based, are synthesized. The aluminium-based MIL-53(Al) and MIL-53-NH_2(Al) are used in polyethylene oxide (PEO) membranes which are characterized by solid-state impedance spectroscopy measurements. The zirconium-based UiO-66 and UiO-66-NH_2 are characterized as well and grafted with various lithium alkoxides. The produced powders are pressed into pellets and soaked with propylene carbonate. The soaked pellets are characterized by impedance spectroscopy in order to evaluate their lithium ion conduction properties.

Zwei unterschiedliche Typen von Metall-organischen Gerüsten, Aluminium- und Zirkonium-basiert, werden synthetisiert. Die Aluminium-basierten MIL-53(Al) und MIL-53-NH_2(Al) werden in Polyethylenoxid (PEO) Membranen verwendet, welche mit Festkörper-Impedanzspektroskopie charakterisiert werden. Die Zirkonium-basierten UiO-66 und UiO-66-NH_2 werden ebenfalls charakterisiert und mit unterschiedlichen Lithiumalkoholaten okuliert. Die hergestellten Pulver werden zu Pellets gepresst und mit Propylencarbonat getränkt. The getränkten Pellets werden mit Impedanzspektroskopie auf ihre Eigenschaften bezüglich der Lithium Ionen Leitfähigkeit untersucht.

2 Introduction

2.1 Metal organic frameworks

Metal organic frameworks (MOF) have been intensely investigated for more than a decade. They can be described as coordination polymers consisting of metal ions connected by organic linkers. This arrangement yields a wide variety of stable, ordered polymers exhibiting a high surface area. The geometry and therefore the size of the generated pores, highly depends on the structure of the used ligand and also on the metal center itself. The ratio between linker and metal center precursor is important, as well as the solvent and an additional source of anions to compensate cations positive charge. During the synthesis, which is usually done by solvothermal reaction, guest molecules, such as the organic linker in excess and solvent molecules, stay in the pores and need to be subsequently removed without damaging the framework. The size of the pores, which can be controlled by the already mentioned variables, is of fundamental significance for the intended application. Possible applications are today centred on gas-storage applications and vapour separation, as a catalyst with high selectivity or as drug storage and delivery. Some of these applications require further modification of the framework with molecules or functional groups, so-called post synthetic modifications (PSM). It is obligatory to use small reagents that can enter the voids of the used MOF and decent reaction conditions to avoid the collapse of the framework [1].

2.2 Metal organic frameworks for lithium ion batteries

Many of the already mentioned advantages of metal organic frameworks make them a promising material for lithium ion batteries. Lithium ion batteries are widely used today, especially in portable equipment. However, there is much to desire in terms of their specific capacity and energy density, an area where improvements are sorely needed. Another major issue is represented by safety aspects. Indeed, the liquid electrolytes used today in all commercial systems are highly flammable and may lead to highly toxic decomposition products, such as HF etc. It would be thus

desired that the commonly used liquid electrolytes are replaced by solid state ionic conductors that are far less exposed to the risks mentioned above [2].

MOFs can be used in all active parts of lithium ion batteries. The cathode for instance, is usually the capacity limiting electrode. Therefore an improvement of the cathode and its intrinsic diffusivity enhances the capacity of the battery and the power density, repectively. MIL-53(Fe), a MOF consisting of Fe(III) clusters linked by terephthalic acid, was the first efficient cathode material synthesized. An electrode consisting of 85 wt% MOF and carbon produced a reversible capacity of $80\,\mathrm{mA\,h\,g^{-1}}$ in the first cycle and showed a capacity retention of 80 % (C/40 to 1C). Issues were reported at a discharge voltage under 0.5 V, when permanent decomposition of the MIL-53(Fe) occurred. Good electrochemical performance and good reversible capacity was also obtained with an organic-phosphate framework. $Li_2[(VO_2)_2(HPO_4)_{1.5}(PO_4)_{0.5}(C_2O_4)]$ has lithium ions diffusion channels and exhibits a reversible capacity as high as $80\,\mathrm{mA\,h\,g^{-1}}$ (25 cycles) [2].

The materials commonly used today as negative electrode (anode) suffer also from similar issues in terms of specific capacity and energy density. The material used today, graphite, shows a specific capacity of just $372\,\mathrm{mA\,h\,g^{-1}}$. The rate performance is low as well. MOF-177, a zinc based framework with 1,3,5-tris(4-carboxyphenyl)benzene as linker, exhibits capacities of $425\,\mathrm{mA\,h\,g^{-1}}$ and $110\,\mathrm{mA\,h\,g^{-1}}$ in the first cycle but collapses because of the lithium insertion [2]. Other diamondoid structured and linked by formic acid frameworks, containing zinc and/or cobalt as metal centres, showed higher robustness as well as thermal stability. The highest reversible capacity was reached with $Zn_3(HCOO)_6$, achieving $560\,\mathrm{mA\,h\,g^{-1}}$ in 60 cycles (0.005 V to 3.0 V). The rate performance was outstanding as well. The suggested, fully reversible mechanism includes the formation of zinc nano particles and lithium formate as well as continuative, reversible conversion to a lithium-zinc alloy [3].

The electrolyte itself, ionically interconnecting cathode and anode, is very important, not only for safety reasons but also for high energy density and power density as well as the inhibition of dendrite growth, should metallic lithium be used or should it occur unwantedly. Liquid electrolytes are a potential risk because they can leak or catch fire easily. Therefore a lot of research is done on solid electrolytes including MOFs soaked with liquids [2]. The most auspicious one is is Mg_2(dodbc) [2]. The mentioned linker of the Mg metal centres is 1,4-dioxido-2,5-benzenedicarboxylate. This structure consists of coordinatively unsaturated Mg^{2+} sites in a honeycomb-type structure, with pores in one dimension. A conductivity of $1.8 \times 10^{-6}\,\mathrm{S\,cm^{-1}}$ at room temperature is reached just by soaking the material with a 1 M solution of $LiBF_4$ in ethylene and diethylene carbonate. An activation energy of 0.31 eV is reported. The post synthetic modification of the framework with grafting of lithium isopropoxide in hexanes to the framework and soaking with

the 1 M solution of $LiBF_4$ demonstrates a conductivity of $3.1 \times 10^{-4}\,S\,cm^{-1}$ and an activation energy of 0.15 eV. The alkoxide anions most likely bind to unsaturated Mg^{2+} sites, letting Li^+ ions move almost freely along the channels [4].

2.3 UiO-66

UiO-66 (UiO = Universitetet i Oslo) consists of a very stable network and can be used in a wide range of conditions, chemical and physical, without collapsing. This robustness makes it an ideal material for post synthetic modifications (PSM) [5]. It consists of secondary building units (SBU) formed by six zirconium cations in an octahedral arrangement, with each linked to μ_3-O and μ_3-OH as well as carboxylate groups. These SBUs show a square-anti-prismatic structure. Each square-anti-prismatic SBU is bridging to twelve other SBUs via the linker. This generates an expanded cubic closed-packed structure (ccp) [6]. This compact structure is generated by in-situ hydrolysis of $ZrCl_4$, linked by terephthalic acid [7]. Through variation of the linker, three structures with analogue geometry can be obtained. In UiO-66, UiO-67 and UiO-68 the Zr-oxo-hydroxo clusters are linked by terephthalic acid, biphenyl-4,4'-dicarboxylic acid or p-terphenyl-4,4"-dicarboxylic acid [6].

The Zr^{4+}-based material is suitable for post synthetic modifications due to its good stability. In the case of UiO-66 this corresponds to the modification of the OH-groups located in the zirconium-cluster. If UiO-66 is heated under vacuum, water can be eliminated from the structure and Zr_6O_6 units are formed. These Zr-sites are coordinatively unsaturated. Therefore, they can be seen as strong Lewis acid. These sites can be grafted with an alkoxide base, while the framework does not collapse. The possible mechanism suggested by Ameloot et al. is shown in figure 2.1 [8]. They expect not more than two grafting sites per $Zr_6O_4(OH)_4(O_2CR)_{12}$. Only 25 % of these sites seem to be occupied experimentally although the ratio of Li^+ to $(tBuO)^-$ is not stoichiometric. Isolated OH groups in the structure have been found to exchange H^+ with Li^+ during the grafting up to 1 Li^+ per cluster. Grafted samples, soaked with 46 wt% propylene carbonate, showed a conductivity of $1.8 \times 10^{-5}\,S\,cm^{-1}$ at room temperature and an activation energy of 0.18 eV. This UiO-66 grafted with lithium tertiary butoxide can be referred to as superionic conductor most likely because the negative charge of the alkoxide is shielded [8].

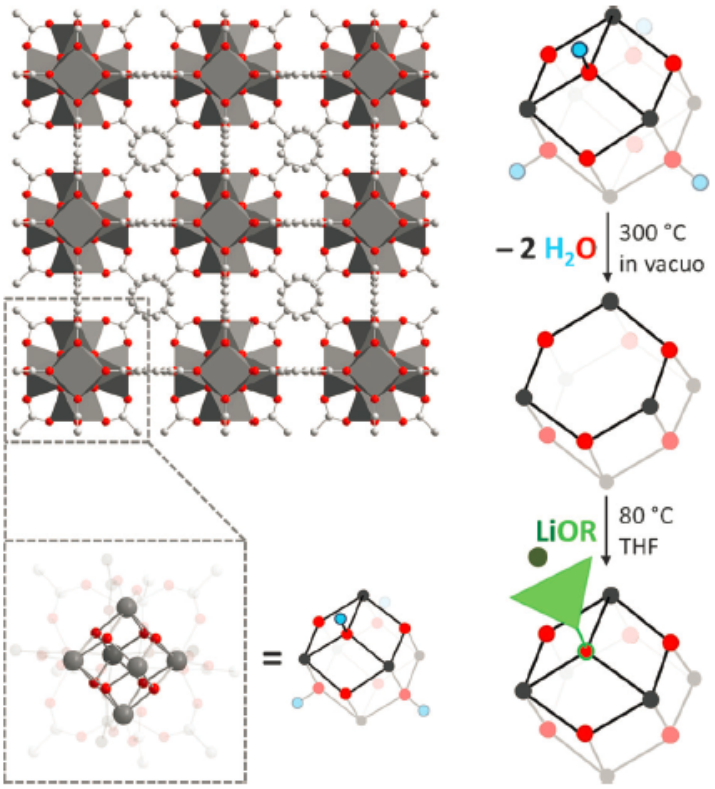

Figure 2.1: Illustration of the grafting process in UiO-66. Zirconium is depicted gray, oxygen red, carbon dark green and hydrogen blue. The crystal structure of the material is shown on the left. On the right, the grafting process is shown. After the dehydration at elevated temperatures, the framework is grafted subsequently with lithium tertiary butoxide, which is pictured by a light green triangle [8, p. 5533].

2.4 MIL-53(Al)

MIL-53 (MIL = Materials of Institute Lavoisier) is one of not more than five crystalline structures formed by a trivalent cation and terephthalic acid. The encoded number represents a recognisable crystal structure. The MIL-53 structure is possible with iron as well as aluminium and other trivalent cations such as chromium. Due to its good structural flexibility it was tested for a range of possible applications such as drug delivery, lithium insertion reactions and liquid-liquid separation [9]. The flexibility of the homologues is recognizable in the strong breathing effect during hydration. This effect is only possible due to the unique crystal structure. The porous aluminium terephthalate MIL-53(Al) consists of $AlO_4(OH)_2$ octahedra.

These are connected to infinite trans chains through the OH groups. Additionally they are interconnected by terephthalic acid. The proposed structure is shown in figure 2.2 [10].

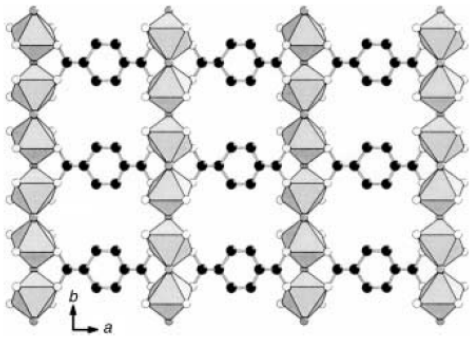

Figure 2.2: Structure of MIL-53(Al). The infinite trans chains connected through terephthalic acid are shown. The octahedra represent $AlO_4(OH)_2$, with aluminum in the centre and hydroxyl groups (gray) interconnecting them [10, p. 1375].

The one dimensional rhombic tunnels are only visible in one direction and are shown in figure 2.3. These tunnels show different dimensions according to the interior filling. Right after the synthesis, the so-called as synthesized form, these pores are filled with excess terepthalic acid and have dimensions of 7.3 Å and 7.7 Å. The crystal structure is an orthorhombic system with Pnma space group. After heating the sample to at least 275 °C, the excess terephthalic acid gets expelled and empty pores stay behind. The crystal structure stays orthorhombic but deforms and the space group changes to Imma. This structure is only stable at high temperatures and is therefore referred to as *ht*. The new pore dimensions are 8.5 Å and 8.5 Å. While cooling to room temperature, the structure adsorbs water. This reversible adsorption deforms the pores even stronger and changes the crystal structure to a monoclinic system with a Cc space group. The pores get flattened to dimensions of 2.6 Å and 13.6 Å through strong hydrogen bonds [10].

The MIL-53(Al) shows a good flexibility in the structure and outstanding behaviour in aqueous solutions of different pH. Investigated from room temperature up to 100 °C the structure does not show any collapse in neutral and acidic media. In basic solutions, however, MIL-53(Al) shows structural changes [11].

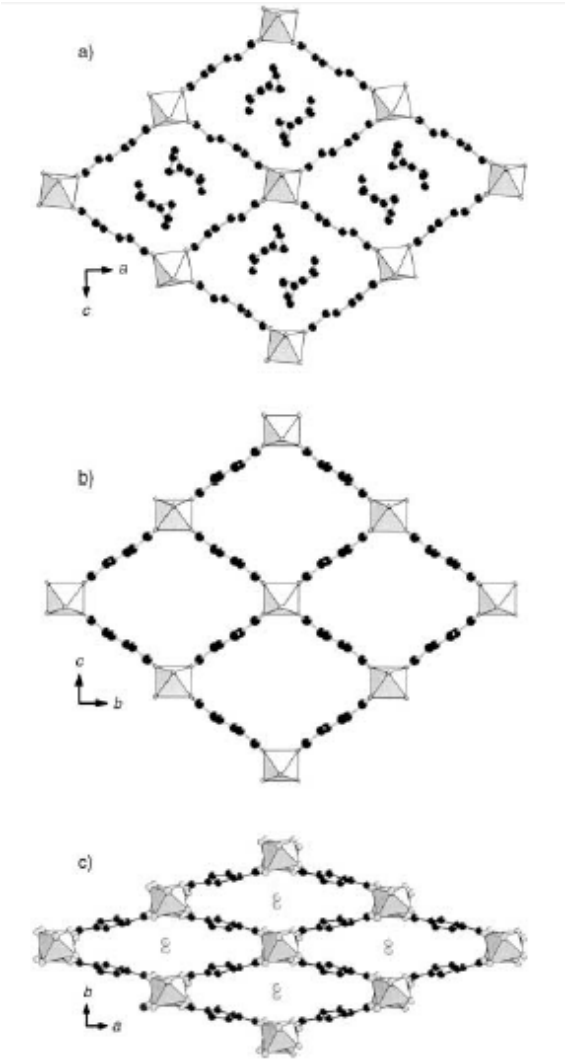

Figure 2.3: Proposed breathing effect in MIL-53(Al) illustrated by the channel system in the framework: a) MIL-53(Al)*as* with occupied channels; b) MIL-53(Al)*ht* with empty channels; c) MIL-53(Al)*lt* with adsorbed water molecules in the channels [10, p. 1374].

3 Experimental

3.1 Zr-based MOFs

3.1.1 Synthesis of UiO-66 and UiO-66-NH_2

UiO-66 and UiO-66-NH_2 were synthesized according to the method of Katz et al. [7]. The initial weights were up-scaled so that a 100 mL screw-cap bottle (Schott) could be used as a reaction vessel. $ZrCl_4$ ($\geq$99.5%, Sigma Aldrich) was put in the bottle and dimethylformamide (DMF; 99.8+%, ACS, Alfa Aesar) and HCl (35%, VWR) were added. The remaining $ZrCl_4$ was dissolved after 20 minutes of ultrasonic treatment. The solution had a greenish colour. Then either terephthalic acid (98%, Sigma Aldrich) or 2-aminoterephthalic acid (99%, Sigma Aldrich) was added as well as additional DMF. It was sonicated again for 20 minutes. The 2-aminoterephthalic acid solution was yellow. Then the bottle was closed with the screw cap and put into a preheated oven at 80 °C over night.

A powder formed and sedimented overnight. The product was filtered over a fine frit (P4, Labor Ochs) and was washed three times with 40 mL DMF and three times with 40 mL of ethanol absolute (>99%, Fisher scientific). The product was dried in a drying oven at 60 °C. Afterwards the UiO-66 and UiO-66-NH_2 were activated by drying at 100 °C under vacuum and then at 120 °C under high vacuum for at least three days. Afterwards, the temperature was slowely increased to 300 °C over 5 hours time. At 300 °C, the initially white powder of UiO-66 started to turn brownish. After 45 minutes at 300 °C, the heat was turned off and the sample was cooled down under high vacuum ($p<5 \times 10^{-6}$ mbar). UiO-66-NH_2 did not show any change in colour. Afterwards the samples were transferred to a glove box, filled with argon (H_2O and O_2 content <1 ppm), and stored there.

3.1.2 Characterization of UiO-66 and UiO-66-NH_2

Before activation the powders were characterized using powder X-ray diffraction and attenuated total reflection (ATR) infra-red spectroscopy. A D8 Advance X-ray diffractometer from Bruker with Bragg Brenanto Geometry was used at room temperature with CuK_α and a LYNXEYE Detector. For IR measurements an Alpha-P spectrometer from Bruker was used.

3.1.3 Grafting on UiO-66 and UiO-66-NH_2

A known mass of activated UiO-66 or UiO-66-NH_2, typically between 100 mg and 250 mg was put in a Schlenk tube. Then, a 1 M solution of alkoxide in tetrahydrofuran (THF) was added. The ratio was 100 mL 1 M alkoxide solution per 1 g of activated MOF. A piece of lithium was put into the female joint cap to act as a getter material for oxygen. The Schlenk tube was closed, taken out of the glove box and the reaction was carried out under continuous stirring and heating on an oil bath at 80 °C for seven days.

Afterwards the Schlenk tube was transferred back to the glove box and the dispersion was transferred into a closed glass vial. It was centrifuged with a Megafuge 1.0 from Heraeus at 2500 rpm for 10 minutes. The sedimented powder was left in the vial and the clear solution was removed with a Pasteur pipette in the glove box. Dry tetrahydrofuran (THF; inhibitor-free, ≥99.9%, Sigma Aldrich) was added and the procedure was repeated five times. Finally, the product was dried under vacuum at 120 °C for 3 hours.

3.1.4 Synthesis of various alkoxides

Four different alkoxides were used. One of them, a 1 M solution of lithium tertiarybutoxide in THF, was purchased from Sigma Aldrich. The other solutions of alkoxides were synthesized according to a patent [12] starting from the corresponding alcohol. The structures of the corresponding alcohols are shown in figure 3.1.

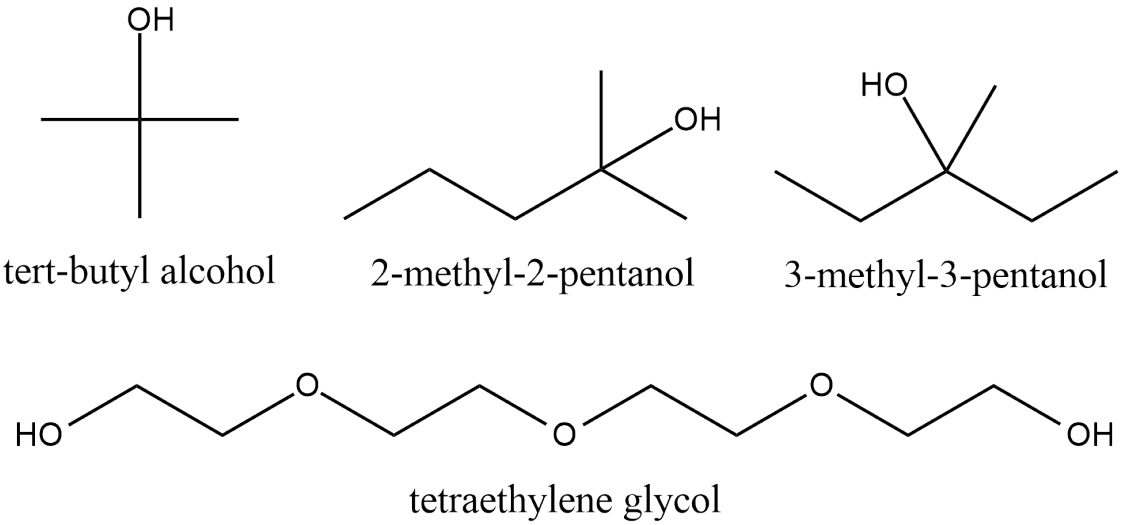

Figure 3.1: Structures of the used alcohols

3-Methyl-3-pentanol (≥99%, Sigma Aldrich), 2-methyl-2-pentanol (99%, Sigma Aldrich) and tetraethylene glycol (99%, Sigma Aldrich) were dried on molecular sieves and stored in the glove box. The glassware for the synthesis was dried at 120 °C and placed hot into the airlock of the glove box in order to minimize the water contamination. Then, pieces of lithium, about 1 cm × 2.5 cm, were cut and their surface was cleaned by scratching with a scalpel until it was shiny. The molar ratio lithium:alcohol was 4:1. The cleaned lithium pieces were put into a three-neck round flask that was closed using Teflon sealing rings. These rings are mandatory. During the first reaction attempt, the THF dissolved the grease from the joints and contaminated the reaction mass. Thus the use of grease for the assembly of the reaction apparatus is not possible. The next steps were performed using the Schlenk-technique. 40 mL of dry THF were added and the stirring was started. Then dry alcohol was added slowly. With tertiary alcohols the reaction started at elevated temperatures, judging from the H_2 evolution. The reaction was held at 68 °C and low argon flow for 3 hours to prevent THF evaporation. The reaction was supposed to be quantitative because H_2-evaporation stopped after a while. The lithium pieces were thinned and pitted after the reaction. The whole, mostly hazy solution was transferred to a volumetric flask and filled to the mark with dry THF so that a 1 M alkoxide solution in THF was obtained.

Tetraethylene glycol did react immediately with the lithium. The solution reached the reflux temperature without additional heating. The H_2 evolution stopped and the reaction mass cooled down. Most of the solution was transferred to a volumetric flask, but a highly viscous residue stayed behind and was not transferred.

3.1.5 Characterzation of grafted UiO-66 and UiO-66-NH_2

Pellets of the powders were pressed using a Specac press, in the glove box under a pressure of 3000 N. The diameter of each pellet was 7 mm. UiO-66, grafted with lithium tert-butoxide, was used for soaking with propylene carbonate (PC, anhydrous, 99.7%, Sigma Aldrich) via the gas phase. Powder, a pellet and an open tube with PC were put into a screw-cap bottle. The bottle was put into an oven and heated to 80 °C, 100 °C and 120 °C, 24 hours each. The oven was cooled down slowly and the evaporated PC condensed. A content of 13.8 wt% PC in the alkoxide-grafted UiO-66 pellet was reached. All other pellets were pressed with 20 µm thick copper foil on one side as contact and mechanical support and the PC was added with a microsyringe (50 µL, Hamilton) on the exposed side.

The soaked UiO-66 powder was sealed in a glass tube and ^{7}Li NMR was carried out, using a Bruker Avance III spectrometer with a shimmed cryo-magnet B_0=7.04 T. The temperature was varied from −60 °C to 50 °C using an Eurotherm controller and a stream of N_2 gas. ^{7}Li NMR spectra at different temperatures

and ^{7}Li spin-lattice relaxation NMR rates ($1/T_1 = R_1$) in the laboratory frame of reference were obtained under static conditions. R_1 rates were recorded with the saturation recovery pulse sequence ($10 * \pi/2 - t_d - \pi/2-$ acquisition). The initial sequence of ten $\pi/2$ pulses was used to erase any longitudinal magnetization M_z. The recovery of $M_z(t_d)$ was reported as a function of the delay time t_d.

Impedance of pressed and soaked pellets was measured using an air tight, laboratory-made Teflon cell and a Concept 80 system (Novocontrol) with an Alpha-A RF impedance analyser and an active ZGS sample cell. The measured frequency ranged from 10 mHz to 10 MHz and the measured temperatures from −65 °C to 65 °C

Two samples, UiO-66 and UiO-66-NH_2, both grafted with lithium tertiary-butoxide, were measured under pressure using the Specac press outside of the glove box with a specially designed insulating pressing die made of PEEK (Polyether ether ketone) polymer. The die was used with the original 7 mm anvils, between which the sample was pressed. The pellets were placed in the press under pressure in the glove box to avoid contamination of air and moisture. The press was connected to the Novocontrol impedance spectroscopy measuring device with copper stripes. All measurements were performed at room temperature (23 °C) and varying pressures.

3.2 Al-based MOFs

3.2.1 Synthesis of MIL-53(Al) and MIL-53-NH_2(Al)

MIL-53(Al) and MIL-53-NH_2(Al) were synthesized according to the method of Loiseau et al. [10]. The initial reactant quantities were up-scaled to a total volume of 60 mL water. The amount of $Al(NO_3)_3 \cdot 9\,H_2O$ (≥98% , Sigma Aldrich) was dissolved in half of the water (milipore). Terephthalic acid (98%, Sigma Aldrich) or 2-aminoterephtalic acid (99%, Sigma Aldrich) was dispersed in the other half of the water. The solution of the aluminiumnitrate was poured to the linker dispersion and mixed for a while. Then the the reaction mass was loaded in a 250 mL Teflon lined autoclave. The autoclave was kept under autogenous pressure at 220 °C for 72 hours for the synthesis of MIL-53(Al) or at 150 °C for five hours for MIL-53-NH_2(Al).

The formed white solid of MIL-53(Al) was filtered over a fine frit and washed with 50 mL water (milipore). The white powder was dried at 60 °C in a drying oven (MIL-53*as*). Most of the powder was placed in a silica crucible inside a tube furnace where the temperature was ramped up with a rate of 2 °C min^{-1}, held at 120 °C for two hours and again ramped up and held at 330 °C for 72 hours with subsequent natural cooling leading to MIL-53*lt*. This procedure removed water and terephthalic acid in the pores of the MOF.

The formed yellowish solid of MIL-53-NH_2 was filtered over a fine frit, washed with water and dried at 60 °C (MIL-53-NH_2*as*) as well. Most of the powder was put into a flask and dispersed in 30 mL of N,N-dimethylformamide (DMF, 99.8+%, Alfa Aesar). The dispersion was held under reflux at 150 °C for half an hour. It was filtered hot over a fine frit and washed with DMF. The product was a little bit brownish and was dried in an open tube furnace at 130 °C over night to remove DMF (MIL-53-NH_2*lt*).

3.2.2 Characterization of MIL-53(Al) and MIL-53-NH_2(Al)

The as synthesized (*as*) and low temperature (*lt*) modification of the products were characterized by X-ray diffraction and attenuated total reflection (ATR) infra-red spectroscopy as described in section 3.1.2 on page 8 as well as by thermogravimetric analysis (TGA).

3.2.3 PEO-membranes with Al-based MOFs

Membranes consisting of polyethylene oxide (PEO, 100.000, Alfa Aesar), $LiClO_4$ and the synthesized MIL-53*lt* and MIL-53-NH_2*lt* were prepared. The amount of dry salt, PEO and MOF were put in a polypropylene beaker under air and acetonitrile

(99.9+%, Alfa Aesar) was added. It was thoroughly mixed with three zirconium balls in a 20 mL beaker using a Pulverisette 7 from Fritsch at 300 rpm three times, 15 minutes each. Afterwards, it was cast on a glass Petri dish and dried under air. A content of 20 mg salt in 1 g solid components could not be exceeded due to observed crystallisation in the dry membrane. LiTFSI could not be used as conducting salt due to its hydrophobic properties and lead to an intercalation of water in the membrane. Casting on Teflon foil was not sufficient as well because the membranes curled strongly.

The amount of used acetonitrile was dependent on the ratio between PEO and MOF. The more MOF was used, the less acetonitrile was needed. Membranes with an amount of 0, 5 and 10 wt% of MIL-53*lt* or MIL-53-NH_2*lt* were prepared. Higher amounts of MOF lead to an increase in phase separation and cracking of the membranes during drying.

3.2.4 Characterzation of PEO-membranes with Al-based MOFs

The membranes without conducting salt and an amount of 0, 5 and 10 wt% of MIL-53*lt* were first characterized using TGA to determine the melting point. Then discs with a diameter of 8 mm were punched from the membranes with conductive salt, including MIL-53*lt* as well as MIL-53-NH_2*lt*. These discs were dried under vacuum at 60 °C for some days to remove any adsorbed water. Afterwards impedance measurements were performed, using a Teflon cell as sample holder and a Concept 80 system (Novocontrol, as described in 3.1.5 on page 10). The temperature was varied from −65 °C to 55 °C.

4 Results

4.1 Zr-based MOFs

4.1.1 Characterization of UiO-66 and UiO-66-NH_2

The synthesized Zr-based MOFs, UiO-66 and UiO-66-NH_2, were characterized using powder X-ray diffraction and ATR-IR.

Powder X-ray diffraction was used to verify that the crystal structure of the synthesized powders corresponds to the structure observed in the literature [7]. The diffractograms of UiO-66 and UiO-66-NH_2 show reflections at the same angle (2Θ), as displayed in the comparison in 4.1. Both MOFs are thus confirmed to have the expected crystal structure. Figures 4.2 and 4.3 show the measured and fitted diffractograms of the synthesized UiO-66 and UiO-66-NH_2. The UiO-66 and UiO-66-NH_2 are isostructural with a cubic unit cell that belongs to the Fm-3m space group. After Rietveld refinement a cell parameter of 20.7 Å was found.

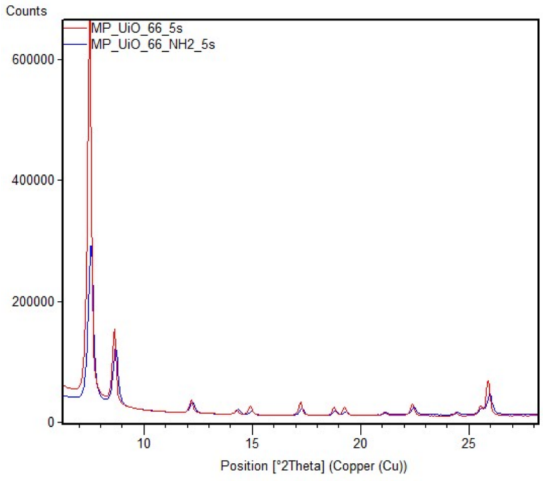

Figure 4.1: Comparison of X-ray diffraction of UiO-66 and UiO-66-NH_2

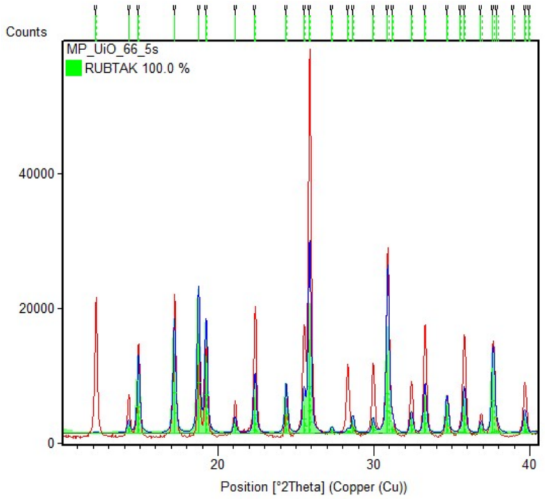

Figure 4.2: X-ray diffraction of UiO-66

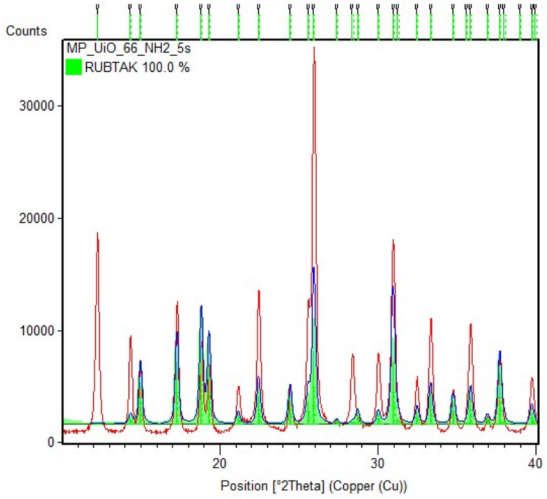

Figure 4.3: X-ray diffraction of UiO-66-NH_2

Although both powders have the same crystal structure, they do not have the same chemical composition. The existence of an amine group in the structure of UiO-66-NH_2 was proven by ATR-IR measurements. In figure 4.4 the spectra of both, UiO-66 and UiO-66-NH_2, are shown. Amine groups usually generate bands of stretching in a range of 3500 cm^{-1} to 3250 cm^{-1} [13]. A weak doublet is characteristic for primary amines (NH_2) and only a single weak band appears for secondary amines (NH). Tertiary amines do not show any band in this range [13]. The spectrum of UiO-66-NH_2 shows a weak broad peak at 3400 cm^{-1}, although amines usually show sharp peaks. Most likely, this broad peak is generated by adsorbed water in the pores due to the measurement conditions in air and moisture. No superposed peak is visible in that range. Therefore, only a tertiary amine is possible in the structure of UiO-66-NH_2. The corresponding medium peak is located at 1257 cm^{-1}. This particular peak does not show up in the IR spetrum of UiO-66 and indicates a tertiary amine in the structure of UiO-66-NH_2.

4.1.2 Characterization of the grafted MOF UiO-66-LitBu

The thermal properties and lithium ion conduction of first synthesized and grafted MOF, UiO-66 grafted with lithium tert-butoxide, were investigated by thermogravimetric analysis and NMR measurements that were performed under inert gas conditions to avoid contamination with air and especially moisture.

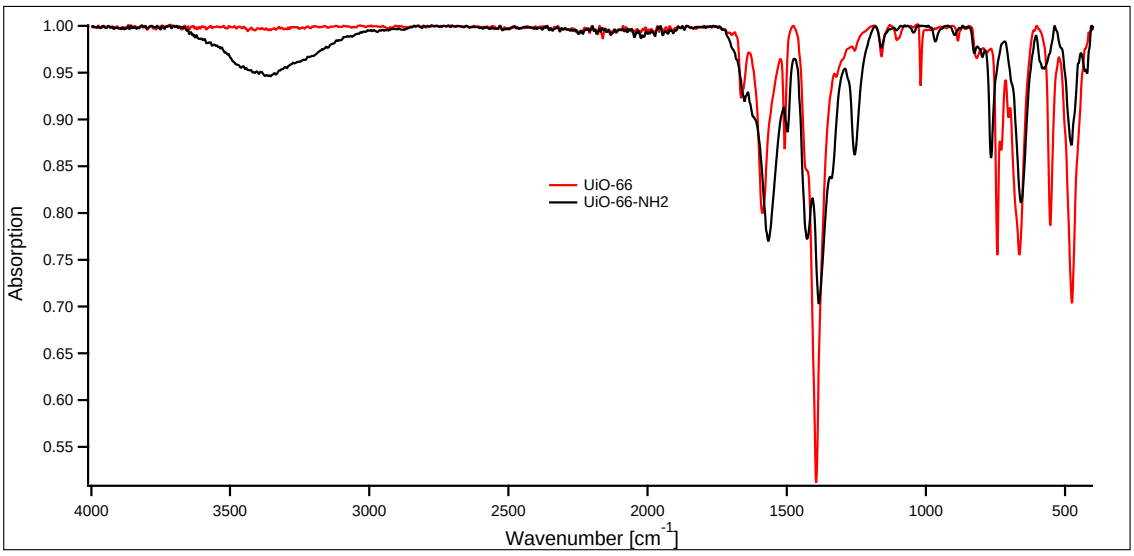

Figure 4.4: ATR-IR spectra of UiO-66 and UiO-66-NH_2

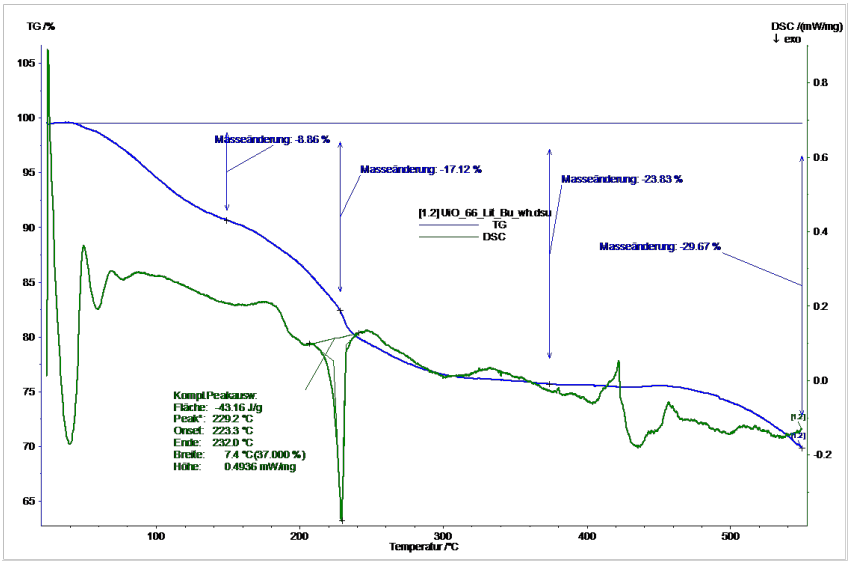

Figure 4.5: Thermogravimetric analysis of UiO-66-LitBu

A loss in weight of 8.9 wt% is observed up to 140 °C, as shown in Figure 4.5. This early loss may be generated by weakly bound alkoxide in the pores. The next loss of 8.3 wt% occurs at 230 °C in an exothermic reaction and reflects the elimination of bound alkoxide in the structure. All of the alkoxide is gone by 300 °C, amounting to a weight loss of 23.8 wt% in total. The structure itself decomposes starting at a temperature of 450 °C by loss of the organic linker.

Also, from the ^{7}NMR spin-lattice relaxation time (T_1) measurements, presented in Figure 4.6, an activation energy of 0.155 eV was found. However, it has to be noted that this activation energy corresponds to a shorter time frame of ionic motion in the sample than for impedance spectroscopy measurements. Therefore, only shorter range lithium ion motion is sensed by T_1 measurements. In accordance with this assumption impedance spectroscopy measurements of the same sample were performed within the same temperature range. The results are shown in Figure 4.7. The conductivity of the sample is quite low and the measured, very low conductivity at low temperatures and low frequencies starts scattering. This low conductivity may be explained by the low amount of propylene carbonate in the pellet that was 13.8 wt% for this very sample. The activation energy derived from the impedance data, shown in Figure 4.8, reaches a value of 0.44 eV which is significantly higher than the value obtained from the NMR measurement. This may be explained if we consider that impedance probes ionic motion over a longer distance range than a T_1 measurement.

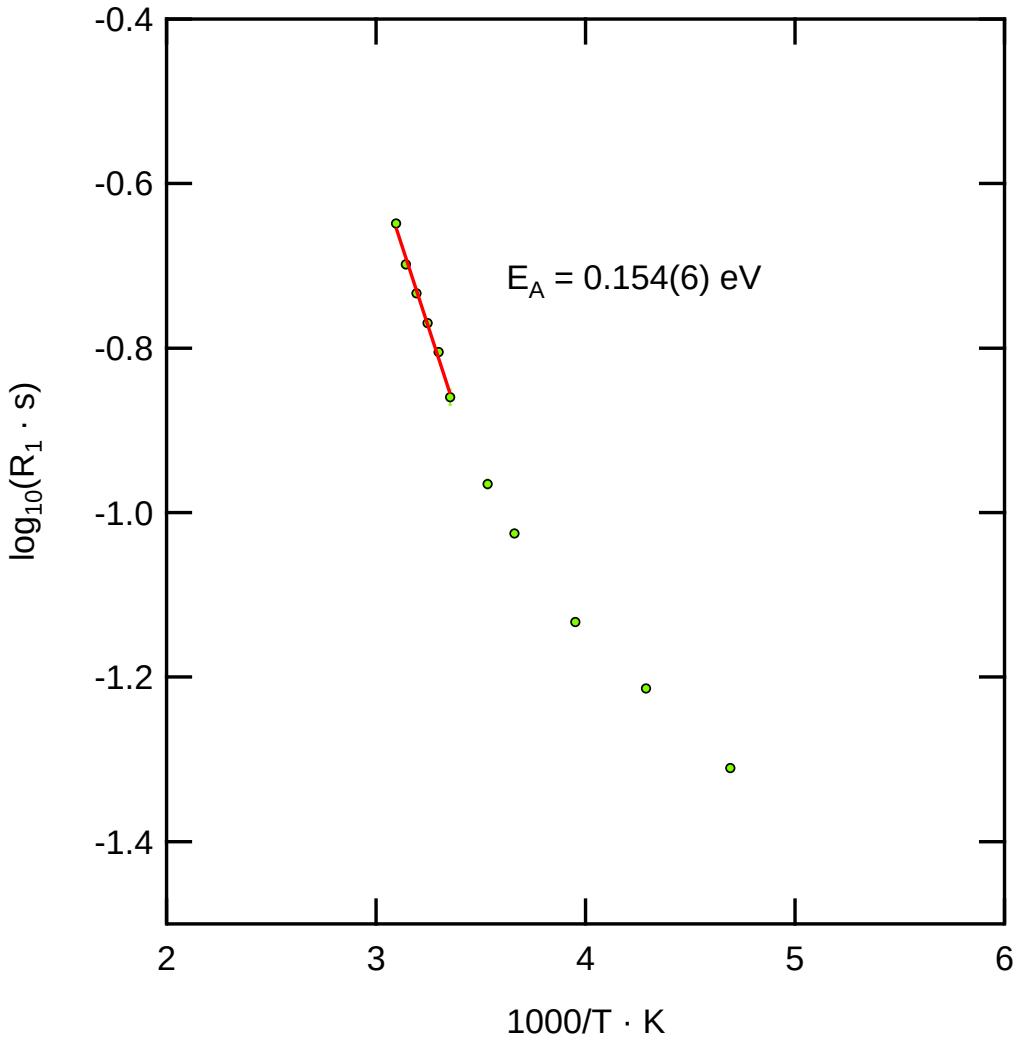

Figure 4.6: ^{7}NMR spin-lattice relaxation rates vs inverse temperature for UiO-66-LitBu with 13.8 wt% propylene carbonate

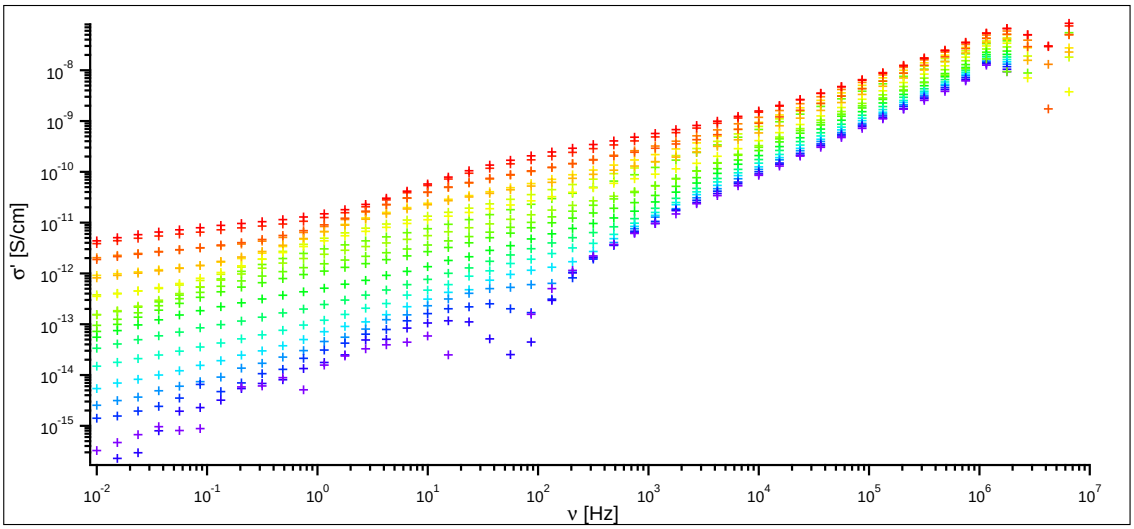

Figure 4.7: Impedance results for UiO-66-LitBu with 13.8 wt% propylene carbonate

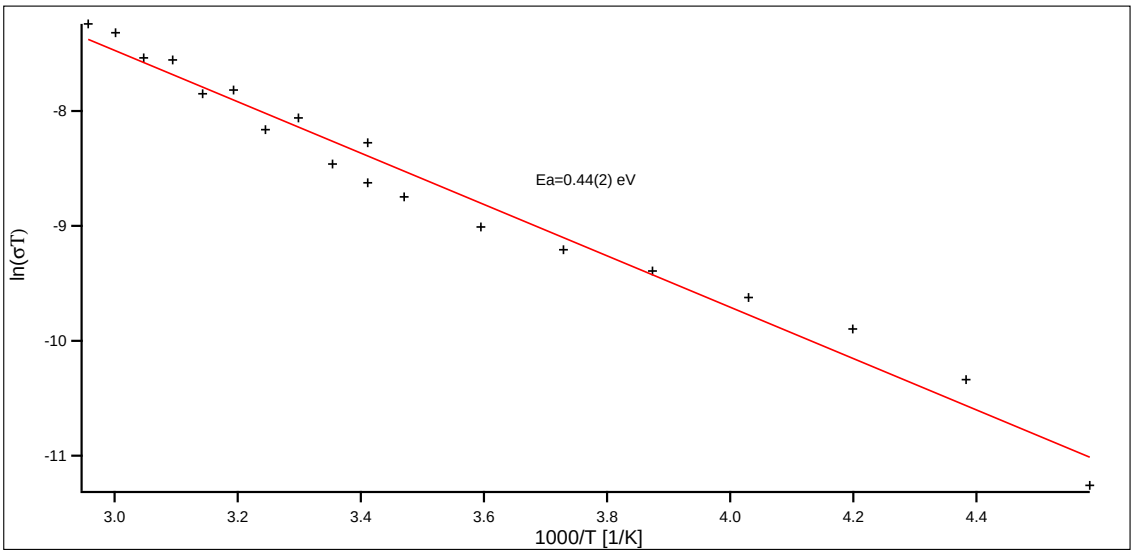

Figure 4.8: Arrhenius plot for UiO-66-LitBu with 13.8 wt% propylene carbonate

4.1.3 Impedance measurements of grafted UiO-66 and UiO-66-NH_2

The impedance spectroscopy measurement results for pellets with a content of 45 wt% propylene carbonate is exemplified in Figure 4.9 for the amine functionalized UiO-66-NH_2, grafted with lithium 2-methyl-2-pentoxide. The plateau of conductivity, also called the DC plateau, is visible over a wide range of frequencies at high temperatures. For low temperatures, two plateaus are visible in that range. Depending on the sample, the second plateau was observed for different numbers of temperatures. Possible explanations for this behaviour can be found in section 4.1.5. To determine the activation energy (E_a), values at the plateau observed at all temperatures were chosen and plotted as Arrhenius plot, like visible in Figure 4.10. The slope of the best-fit line is defined as the activation energy over R, the universal gas constant. This procedure was done for all impedance spectroscopy measurements and the results are compared subsequently. The graphs for all samples are shown in the appendix.

The conductivities of grafted UiO-66 samples at 60 °C are shown in Figure 4.11, while the activation energies are presented in Figure 4.12. The conductivites of the samples at 60 °C vary strongly. The samples grafted with lithium tertiary-butoxide and lithium 2-methyl-2-pentoxide are the lowest, followed by lithium 3-methyl-3-pentoxide. UiO-66 grafted with lithium tetraethylene glycol has the highest conductivity by far. Tetraethylene glycol may be a good grafting agent due to its high

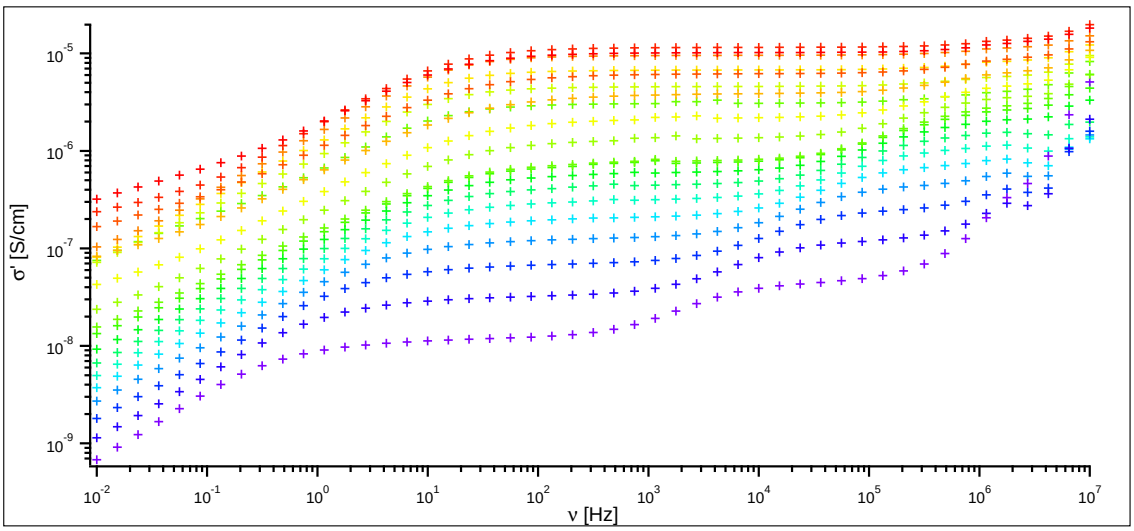

Figure 4.9: Impedance results for UiO-66-NH_2 grafted with Li-2m2p and 45 wt% propylene carbonate

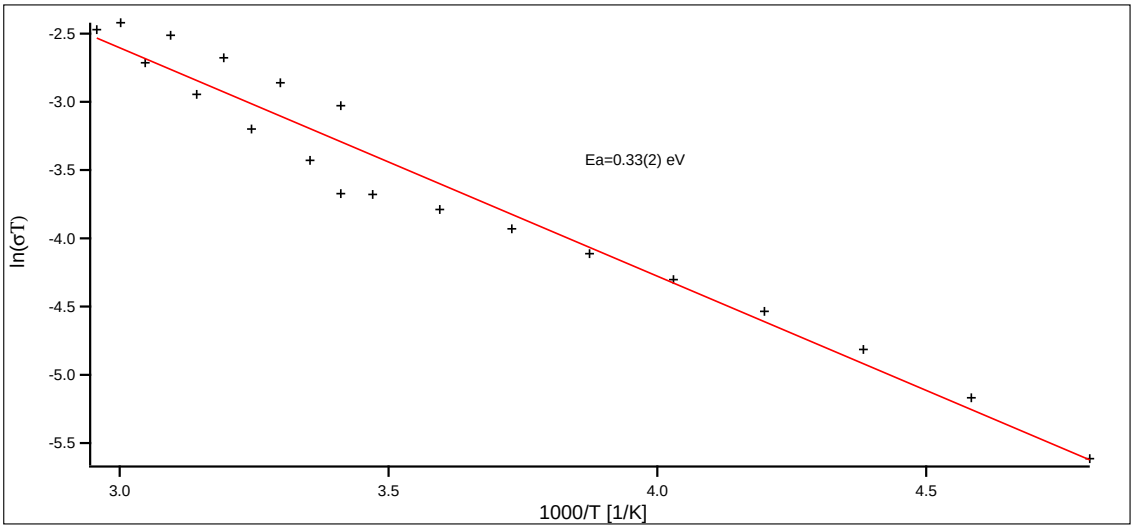

Figure 4.10: Arrhenius plot for UiO-66-NH_2 grafted with Li-2m2p and 45 wt% propylene carbonate

reactivity with lithium and the possibility of two lithium per molecule. Additionally tetraethylene glycol has oxygen bound in the aliphatic chain which may help coordination of the alkoxide to the dehydrated UiO-66 through its lone pairs. Also the activation energy, shown in Figure 4.12 is the lowest for this kind of grafted UiO-66. Most notably in this figure is the high activation energy for the UiO-66 grafted with lithium tertiary-butoxide. All other samples grafted with tertiary alkoxides have lower activation energies. This stands for a stronger coordination of the lithium in the tertiary-butoxide than in others and therefore a higher energy is needed to activate the lithium conduction through the sample.

This effect also occurs in the sample of UiO-66-NH_2 grafted with lithium tertiary-butoxide. The conductivity at 60 °C is low, Figure 4.13, and the activation energy is high, Figure 4.14. In case of the the grafted UiO-66-NH_2 samples, the grafting with lithium 3-methyl-3-pentoxide gives outstanding good properties. The conductivity at 60 °C is much higher than the average and the activation energy is low as well. The sample grafted with lithium tetraethylene glycol still shows a medium activation energy and a medium conductivity. It is not clear how the grafting works in amine functionalized UiO-66 but lithium 3-methyl-3-pentoxide seems to offer a favourable coordination in the framework.

The amine functionalized grafted samples of UiO-66-NH_2 exhibit generally a better conductivity than UiO-66 samples. The amine group might help in a stronger coordination of the alkoxide, letting the lithium ions more freely to move.

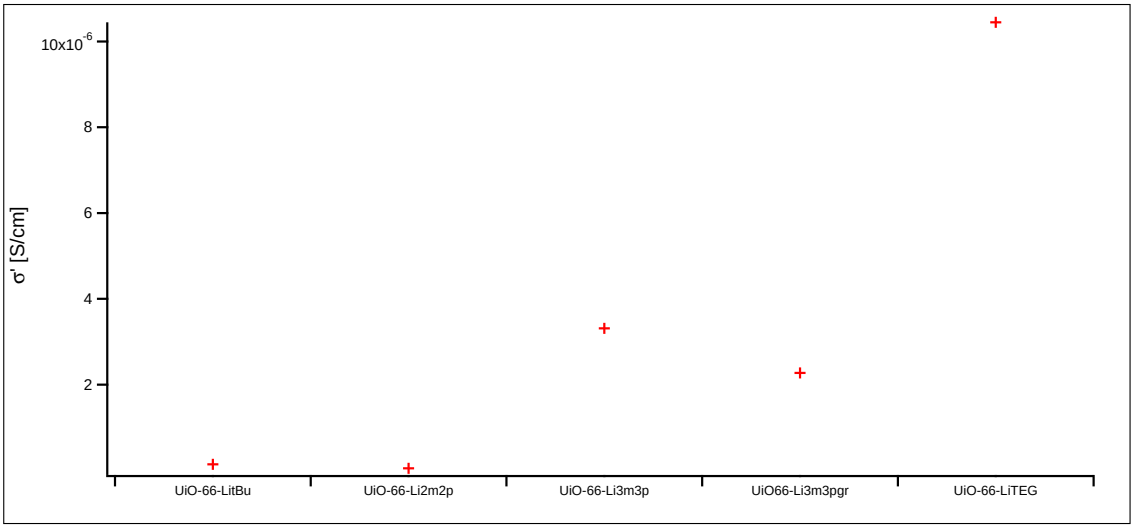

Figure 4.11: Impedance results for grafted UiO-66 samples with 45 wt% propylene carbonate at 60 °C

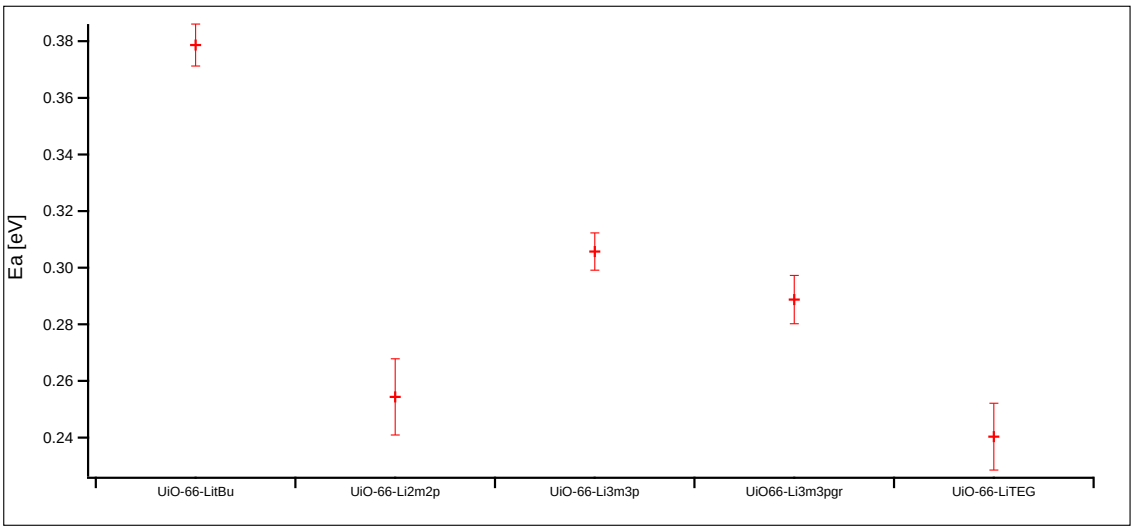

Figure 4.12: Comparison of activation energies for grafted UiO-66 samples with 45 wt% propylene carbonate

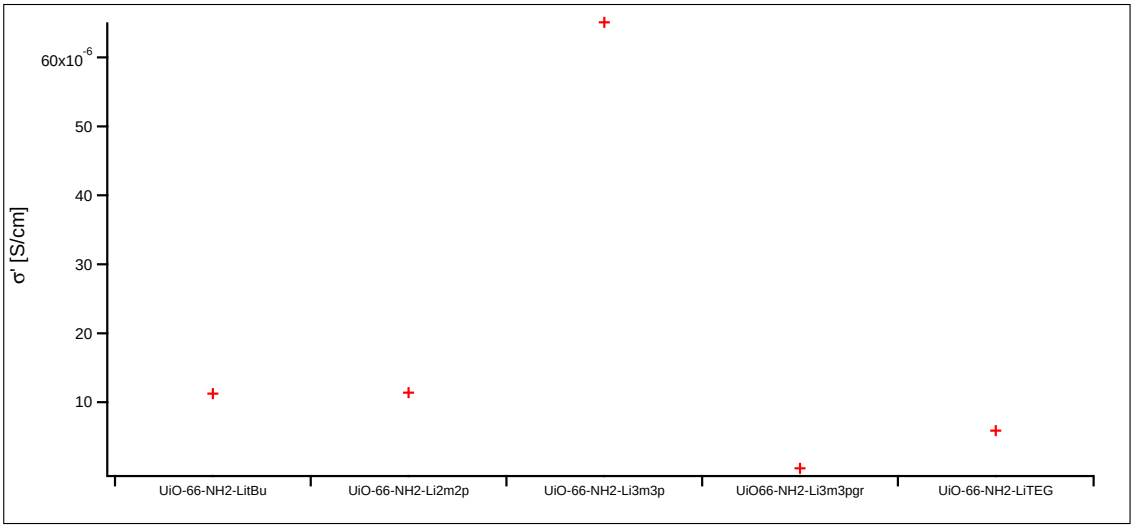

Figure 4.13: Impedance results for grafted UiO-66-NH_2 samples with 45 wt% propylene carbonate at 60 °C

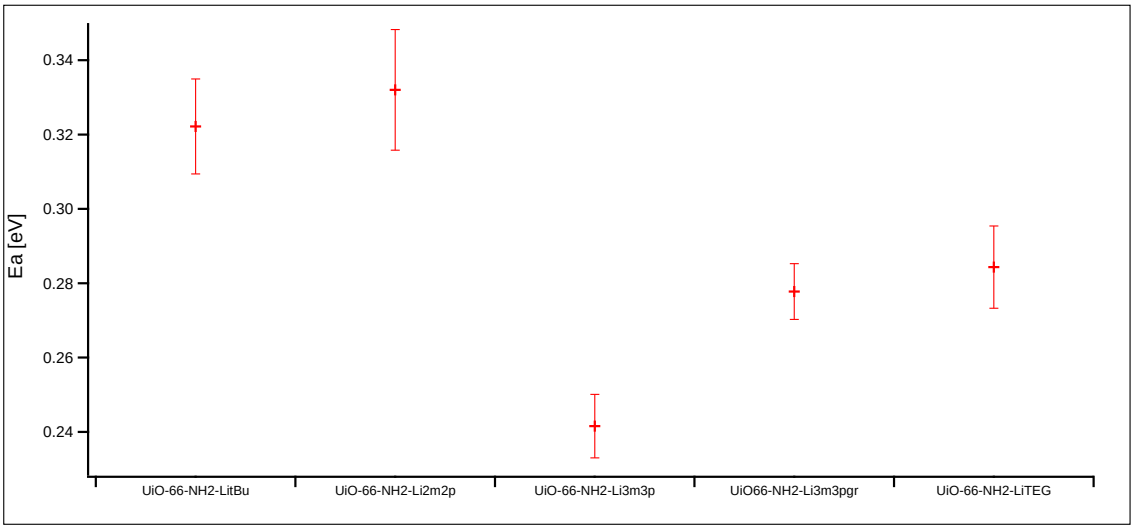

Figure 4.14: Comparison of activation energies for grafted UiO-66-NH_2 samples with 45 wt% propylene carbonate

4.1.4 Impedance measurements of selected samples under pressure

UiO-66 grafted with lithium tertiary-butoxide and UiO-66-NH_2 grafted as well with lithium tertiary-butoxide were measured using the Specac press with a diameter of 7 mm outside of the glove box. This measurement was done to check the influence of increasing pressure on the conductivity of the pellet. Both samples were measured starting at 3000 N, the pressure used for pressing the pellets, and up to 9000 N. Then the pressure was released gradually.

UiO-66 grafted with lithium tertiary-butoxide, results are presented in Figure 4.15, shows a very interesting distribution of conductivities among the different pressures. The conductivity stays constant until a pressure of 9000 N is reached. At that pressure the conductivity increases drastically and starts scattering a lot. Probably, this can be observed due to the fact that the pellet was very thin and there was direct contact between the steel parts and the copper foil support of the pellet. The thickness of the pellet without the copper foil was just 0.208 mm. There were also problems fitting the soaked pellet into the press. The pellets do expand a little bit during soaking and therefore need to be forced into the pressing set made of steel. The copper foil does not expand and can be placed easily. The release of the pressure instantly gave the low conductivity again which means that no irreversible change in the pellet occurred through pressure. Therefore a direct contact between the steel parts and the copper foil is most likely, especially because no dispersive regime is visible in the figure at this pressure.

With UiO-66-NH_2 grafted with lithium tertiary butoxide a different behaviour can be observed, Figure 4.16. In this case the initial conductivity is the highest at 3000 N and decreases with the appliance of more pressure. Notable that the conductivity stays at that level also after the release of the pressure back to 3000 N. Therefore an irreversible change in the pellet did occur. This loss in conductivity was likely caused by squeezing the added propylene carbonate out of the pores of the pellets. During the release of the pressure only a small part of the propylene carbonate could the soaked up again because the major part was lost since it just spread all over the pressing set at high pressures.

Summing up, the application of pressure on grafted UiO-66 and UiO-66-NH_2 did not generate the expected strong increase in conductivity. The observed conductivity, however, was much higher at 3000 N and room temperature than the conductivities measured in the air tight cell at that temperature. The increase of pressure on the soaked pellet therefore increases the conductivity to some extent. No second plateau was observed at room temperature.

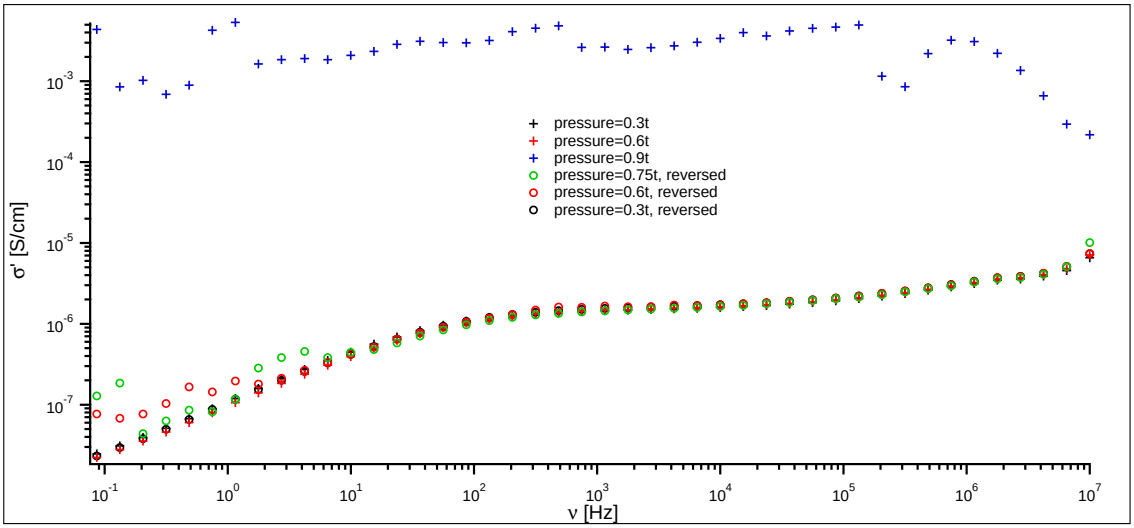

Figure 4.15: Impedance results for UiO-66-LitBu under pressure

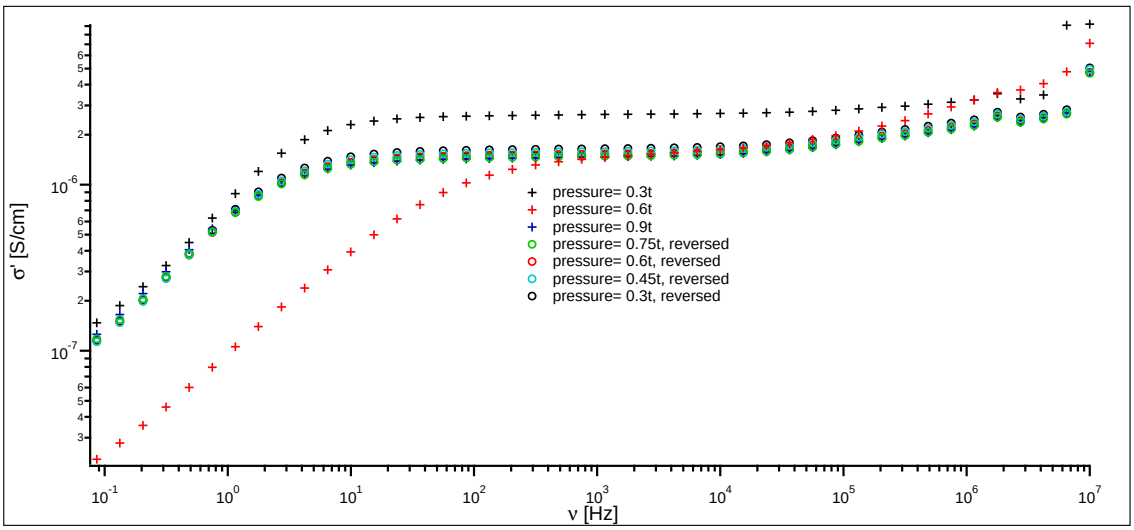

Figure 4.16: Impedance results for UiO-66-NH_2-LitBu under pressure

4.1.5 Capacitative behaviour of grafted UiO-66 and UiO-66-NH_2 samples

The fitting of the impedance data was done exemplarily for the UiO-66-NH_2 sample grafted with lithium 3-methyl-3-pentoxide because it exhibits the second plateau at all measured temperatures. The Nyquist plot including the fit for $-65\,°C$ is shown in Figure 4.17. Especially the positive part of the imaginary impedance is intriguing. Both semicircles were fitted using a constant phase element and a Warburg element (short) for the line. The equivalent electric circuit is shown in Figure 4.18. The constant phase element (CPE) represents a complex impedance when the phase angle is not dependent on the frequency. Therefore it describes the divergence from an ideal capacitance behaviour due to irregularity or roughness of the sample [14].

$$Z(CPE) = \frac{1}{T \cdot (j\omega)^{\phi}} \tag{4.1}$$

Where T is the double-layer capacitance quantity, j is a complex number, ω the angular frequency and ϕ a value smaller than 1. If ϕ converges to 1, an ideal capacitative behaviour can be observed. If it converges to 0, a pure resistor is realized [14].

The capacitance T and the exponent ϕ were determined by fitting at all temperatures for this sample. For the first semicircle, a negative capacitance was observed and monitored, as seen in Figure 4.19. An overall trend is visible. The negative capacitance T increases with temperature, while the exponent ϕ decreases, Figure 4.20.

The same behaviour can be observed for the second semicircle with a capacitance in the positive range, visible in Figures 4.21 and 4.22. The values of the exponent ϕ are somewhat smaller than for the first semicircle. Therefore the general behaviour of this fitted constant phase element shows a bigger deviation from an ideal capacitor than the first semicircle.

Negative capacitance can be observed in a wide variation of samples and was detected especially in semiconductor devices. They are often referred to as instrumental problems being parasitic inductance or insufficient equipment calibration [15] but have been also reported in ferroelectric materials more recently. The capacitance for these materials shows negative values in the barrier region $Q_F = 0$, as presented schematically in Figure 4.23. Due to an applied voltage, the energy scenery and the nearest local minimum is shifted. The polarization favours the lowest possible energy level. If the coercive voltage V_c is reached and exceeded,

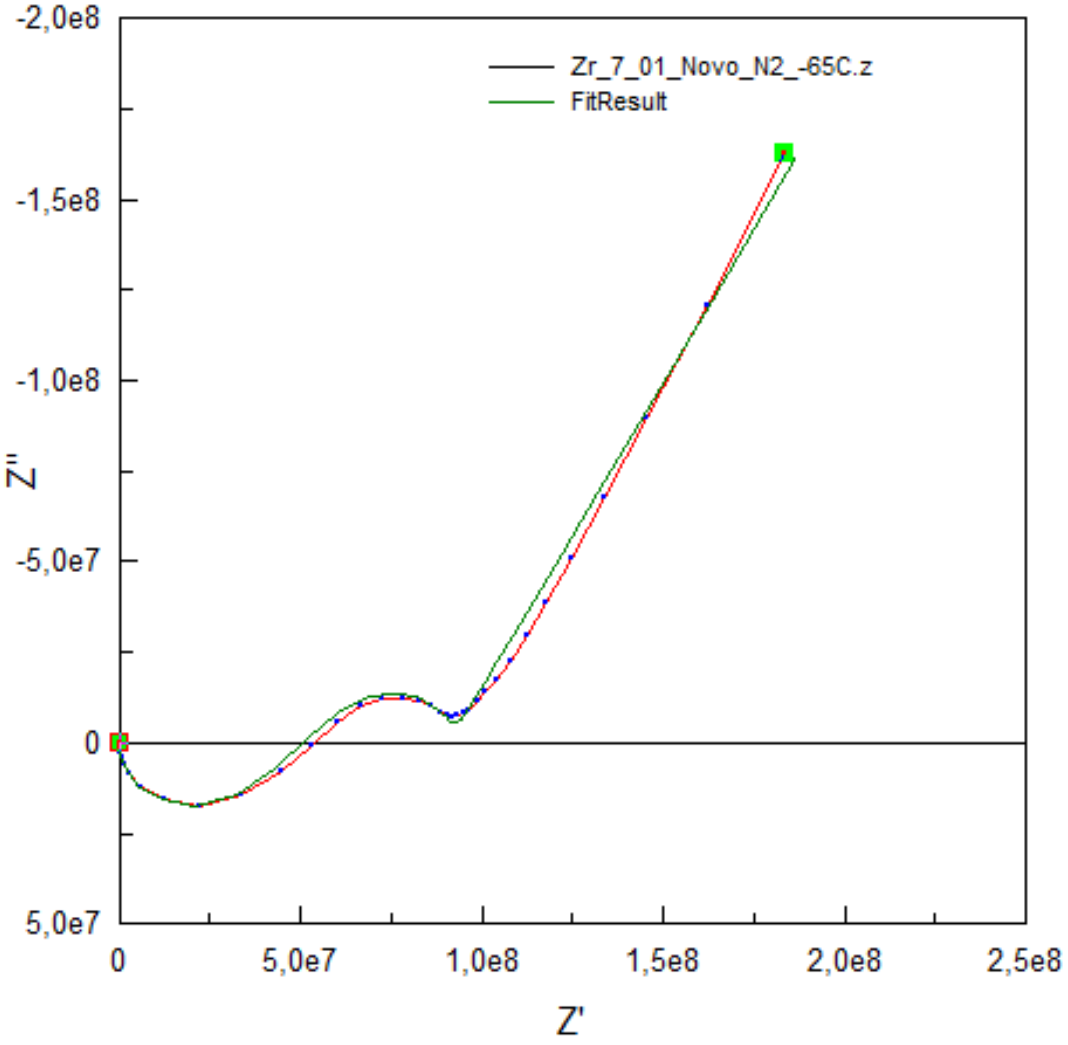

Figure 4.17: Nyquist plot for UiO-66-NH_2 grafted with lithium 3-methyl-3-pentoxide

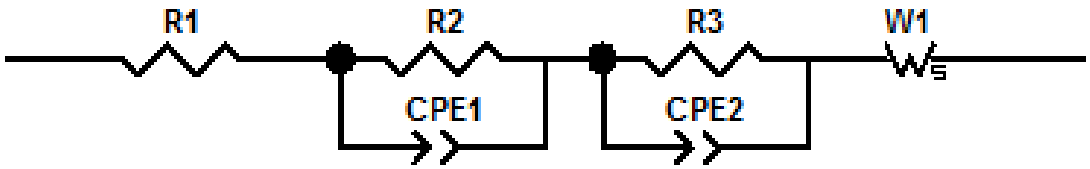

Figure 4.18: Equivalent electric circuit model for UiO-66-NH_2 grafted with lithium 3-methyl-3-pentoxide

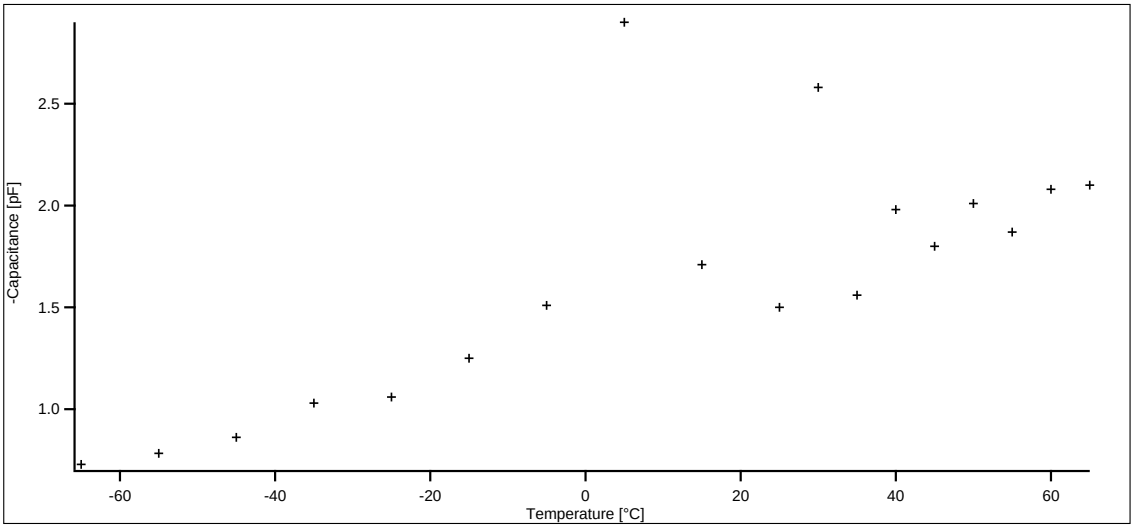

Figure 4.19: Negative capacitance T for the first semicircle over the temperature range

the energy barrier disappears and the given charge relocates itself to the next local minimum. In the process of changing polarization states, it permeates the sector of negative capacitance. The change between two stable states is therefore linked to a negative differential capacitance [16].

Therefore, a possible ferroelectric behaviour might have been observed in the grafted samples due to the negative capacitance.

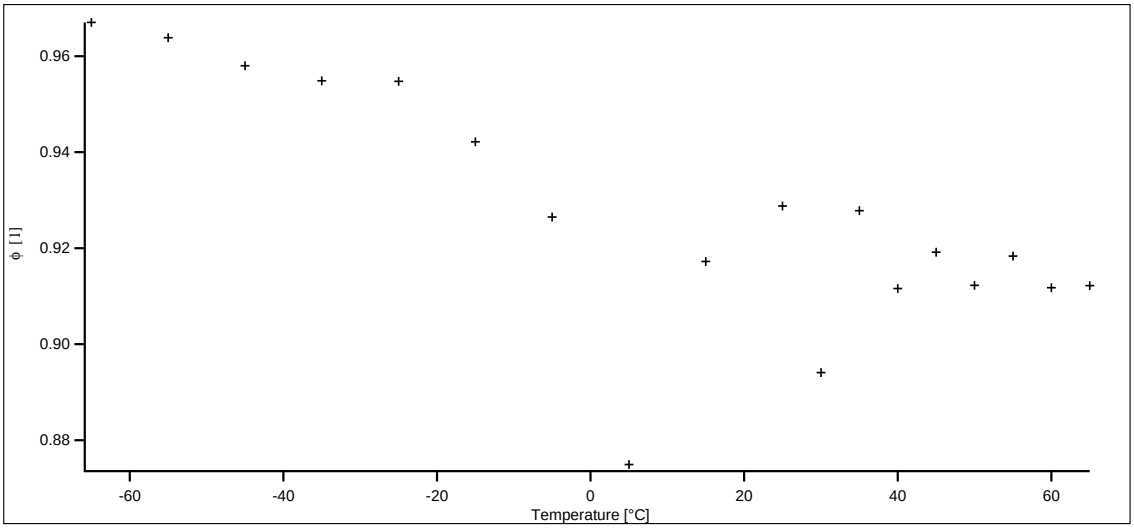

Figure 4.20: Exponent ϕ for the first semicircle over the temperature range

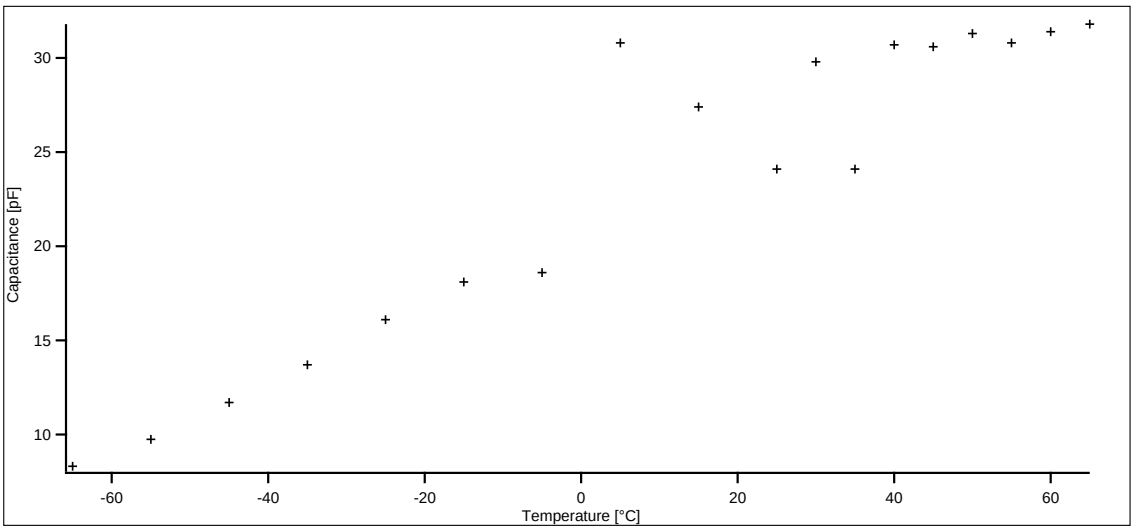

Figure 4.21: Capacitance T for the second semicircle over the temperature range

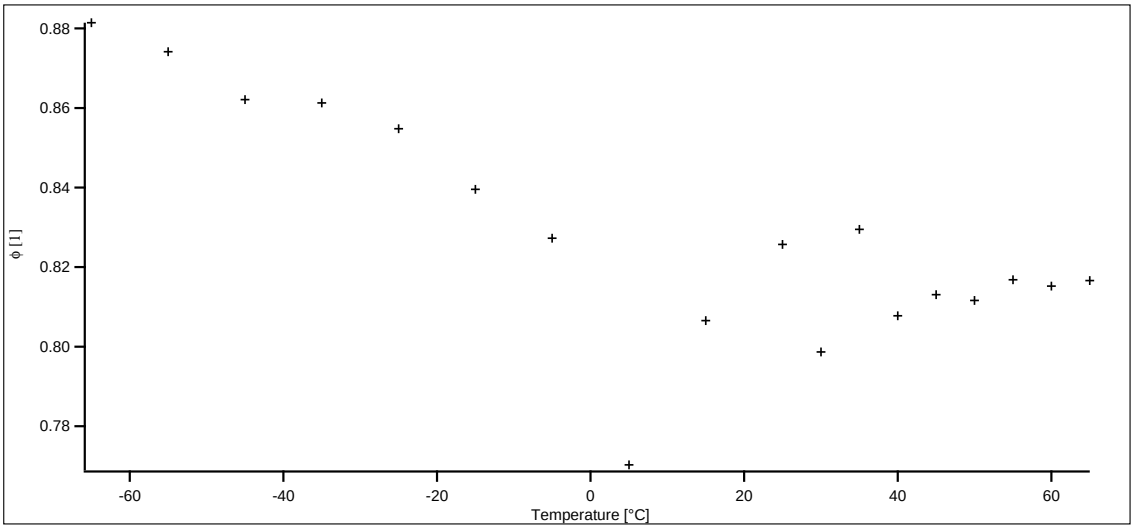

Figure 4.22: Exponent ϕ for the second semicircle over the temperature range

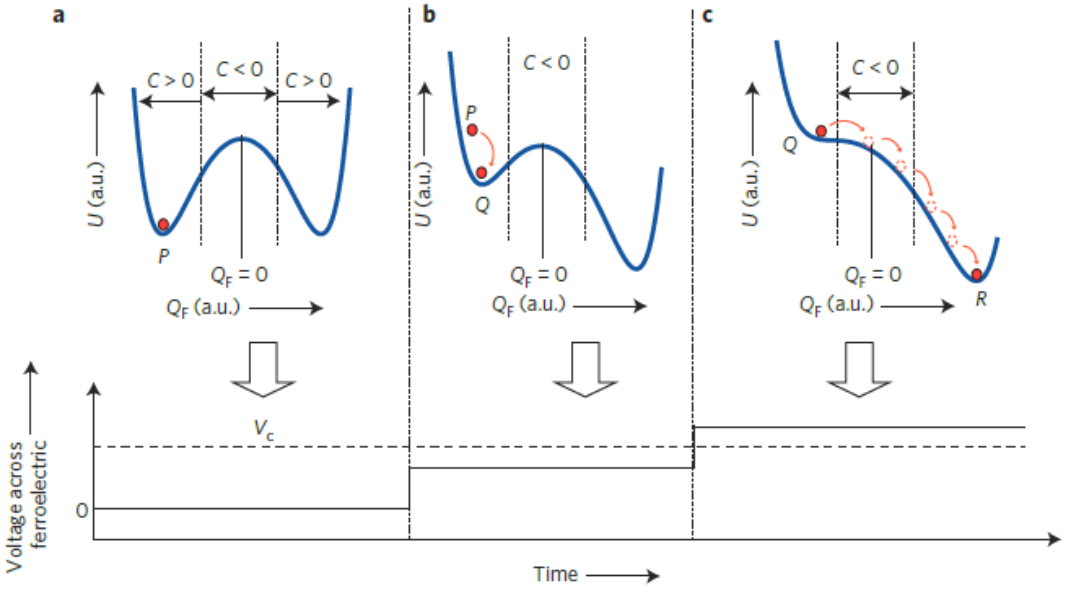

Figure 4.23: Energy scenery for a ferroelectric material: a) If no voltage is applied, negative capacitance (C) is only observable at the maximum of potential energy (U); b) If the applied voltage is smaller than the coercive voltage V_c the local maximum is still present; c) If the applied voltage is greater than V_c the local maximum disappears and the polarization permeates the sector of negative capacitance [16, p. 183].

4.2 Al-based MOFs

4.2.1 Characterization of MIL-53 and MIL-53-NH_2

Both, the as synthesized and low temperature forms of MIL-53(Al) and MIL-53-NH_2(Al) were characterized using powder X-ray diffraction as well as ATR-IR and thermogravimetric analysis. The crystal structures of MIL-53*as* and MIL-53*lt* as shown in Figures 4.24 and 4.25 are composed of two crystal phases each. MIL-53*as* consists mostly of an orthorhombic crystal system with the space group Pnma with unit cell lengths of 17.1 Å, 6.6 Å and 12.3 Å. The minor phase represents a monoclinic crystal system with the space group Cc. The portion of this phase increases due to heat treatment as well as the formation of another orthorhombic phase with Imma space group. The monoclinic crystal system has unit cell lengths of 19.5 Å, 7.6 Å and 6.6 Å as well as angles of 90°, 104.2° and 90°. The other major orthorhombic phase with an Imma space group shows unit cell lengths of 6.6 Å, 16.7 Å and 12.8 Å. Therefore the heat treatment of MIL-53*as* does not only remove water and terephthalic acid but also causes a transition of the crystal phases.

The powder X-ray diffraction of MIL-53-NH_2*as* and MIL-53-NH_2*lt* show mostly one crystal phase. The synthesized MIL-53-NH_2*as*, the X-ray diffractogram is shown in Figure 4.26, has an orthorhombic crystal system with a Pnma space group. It shows the same crystal structure as the major part of MIL-53*as* but with a different organic linker. The unit cell lengths differ as well. For MIL-53-NH_2*as* the unit cell lengths are 16.9 Å, 6.7 Å and 12.6 Å.

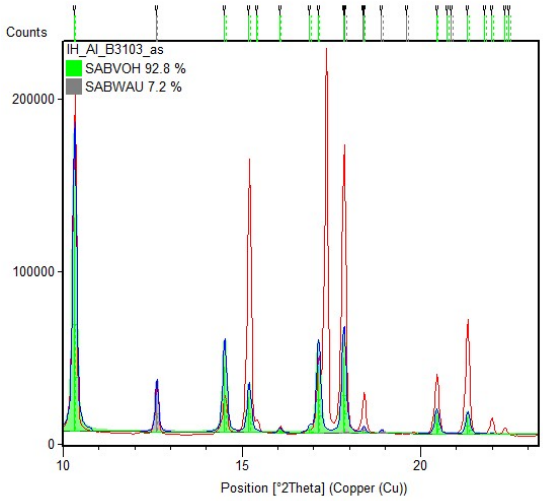

Figure 4.24: X-ray diffraction of MIL-53(Al) as synthesized

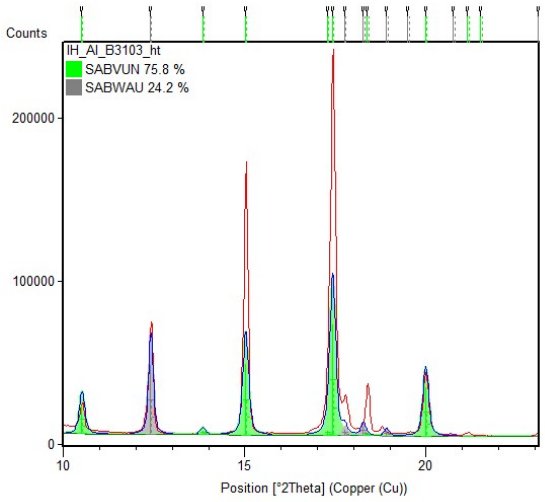

Figure 4.25: X-ray diffraction of MIL-53(Al) after heat treatment

After the heat treatment the Rietveld refinement analysis gives mostly a monoclinic cell with Cc space group for MIL-53-NH_2*lt*, shown in Figure 4.27. This phase represents the low temperature phase of MIL-53(Al). There are also some unassigned reflections that may represent impurities or deformed cells but do not represent the high temperature crystal structure which was also found in MIL-53*lt* in Figure 4.25.

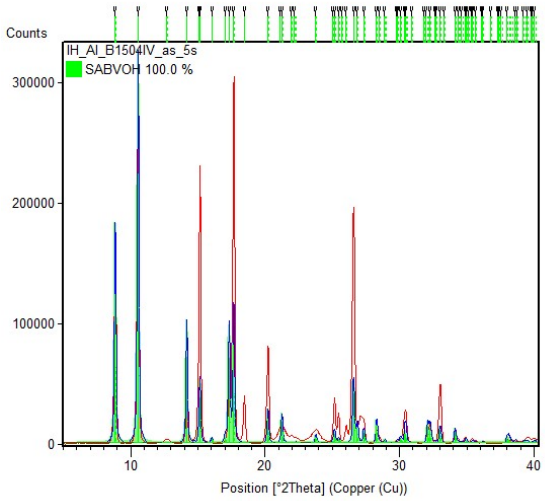

Figure 4.26: X-ray diffraction of MIL-53-NH_2(Al) as synthesized

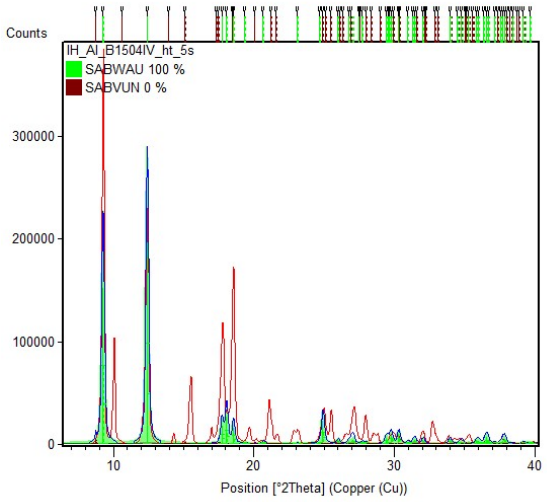

Figure 4.27: X-ray diffraction of MIL-53-NH_2(Al) after heat treatment

The removal of terephthalic acid by the heat treatment was confirmed by ATR-IR measurements. The comparison of the spectra of MIL-53*as* and MIL-53*lt* are shown in Figure 4.28. The weak but sharp bands at 3678 cm^{-1} in MIL-53*as* and 3616 cm^{-1} in MIL-53*lt* belong to OH stretching in the crystal structure. These bands are not broad because the OH-group is sterically hindered and therefore does not form any hydrogen bonds. The broad band observed in MIL-53*lt* at 3455 cm^{-1} reflects the hydrogen bonded stretch of OH-groups due to the water adsorption in the pores after the removal of terephthalic acid. This is confirmed by the C=O stretching vibration of carboxylic acid salt at 1699 cm^{-1} which only occurs in the spectrum of MIL-53*as* but does not occur in MIL-53*lt* after heat treatment.

The amine functionalized MIL-53-NH_2 in Figure 4.29 shows a primary aliphatic amine in both spectra, in the as synthesized as well as in the low temperature form. The weak NH_2 doublet at 3496 cm^{-1} and 3386 cm^{-1} is generated by the out-of-phase and in-phase NH_2 stretching vibrations [13]. The removal of the 2-amino terephthalic acid could not be observed as distinctive as in Figure 4.28.

The thermogravimetric analysis of MIL-53 and MIL-53-NH_2 was performed up to 550 °C. In Figure 4.30 the analysis of MIL-53*as* is shown. The endothermic weight losses at 315 °C, 390 °C and 437 °C correspond to a total loss in 41.8 wt% of the initial weight. These losses indicate the evaporation of terephthalic acid from the pores of the structure because the MOF itself is stable up to 500 °C.

After heat treatment of MIL-53*as* the terephthalic acid in the pores vanished and MIL-53*lt* is formed. The thermogravimetric analysis of the low temperature form

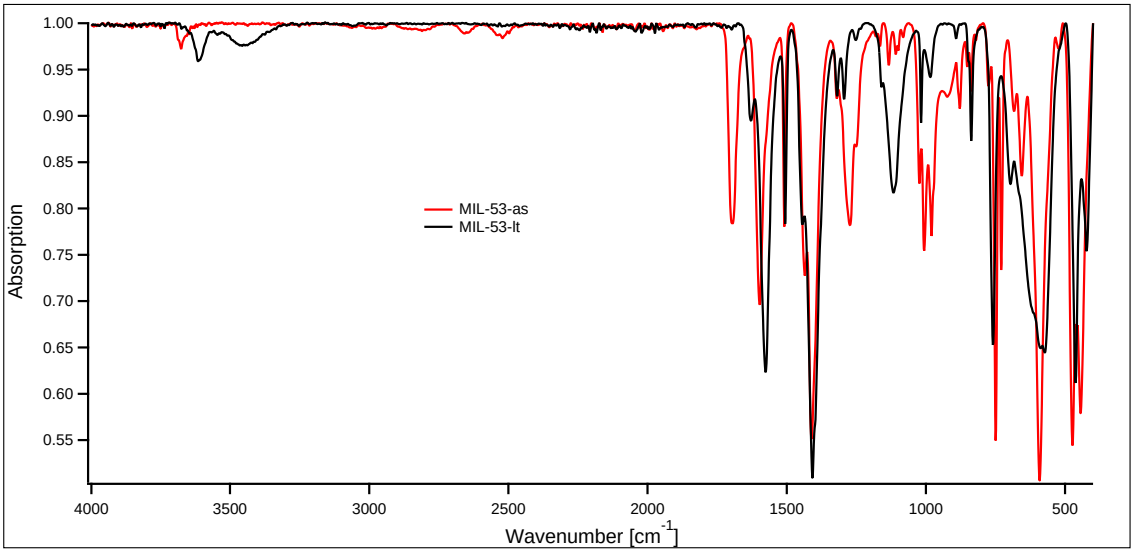

Figure 4.28: ATR-IR spectra of MIL-53*as* and MIL-53*lt*

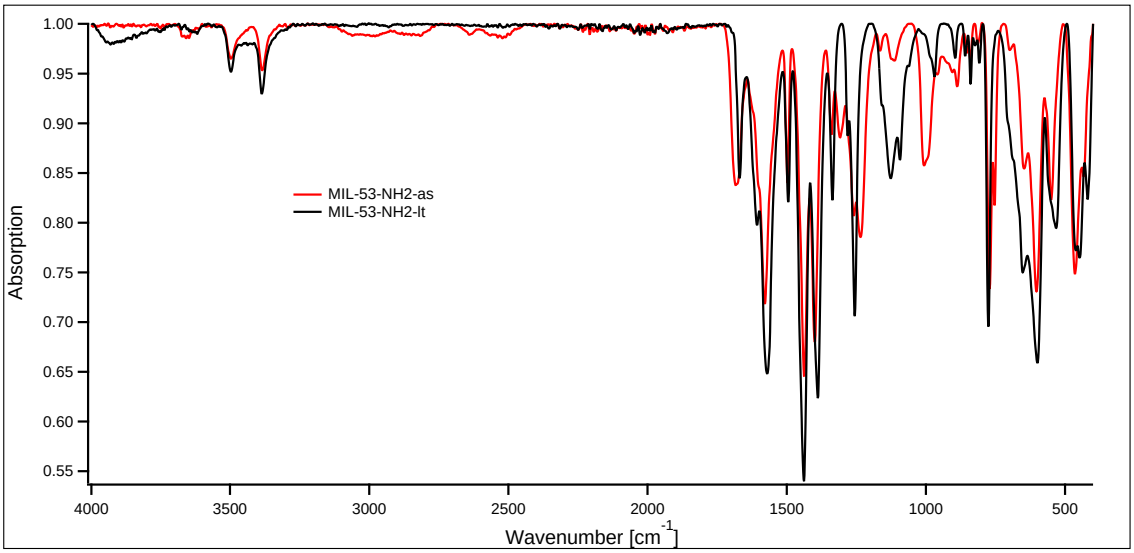

Figure 4.29: ATR-IR spectra of MIL-53-NH_2*as* and MIL-53-NH_2*lt*

in Figure 4.31 shows no gravimetric loss until 500 °C, when the decomposition of the material starts.

The amine functionalized MIL-53-NH_2 on the other hand shows less steps in weight loss. The as synthesized form in Figure 4.32 shows endothermic weight loss at 322 °C with a loss of 24.5 wt%. This step indicates the evaporation of 2-amino terephthalic acid in the pores of the MOF. A loss of 22.8 wt% at 529 °C, however, already indicates the decomposition of the material.

The low temperature form, MIL-53-NH_2*lt*, formed after treatment with DMF, shows no free 2-amino terepthalic acid in the pores any more, Figure 4.33. However, the thermogravimetric analysis indicates DMF in the pores, which could not be removed by the used heat treatment. The endothermic losses of weight are at 210 °C and 512 °C, which belong to the evaporation of DMF (13.8 wt%) located in the pores of the MOF and the starting decomposition of the material (27.3 wt%).

4.2.2 Characterization of the PEO membranes

The PEO-membranes with up to 10 wt% MIL-53*lt* were characterized with thermogravimetric analysis. The aim was to check the influence of increasing MOF content on the thermal behaviour of the PEO membrane.

As seen in Figure 4.34, the membrane with a content of 10 wt% MIL-53*lt* shows an endothermic peak at 66.5 °C which indicates the melting of the membrane. This corresponds to the melting point of the PEO membrane with no MOF inside, 66.1 °C.

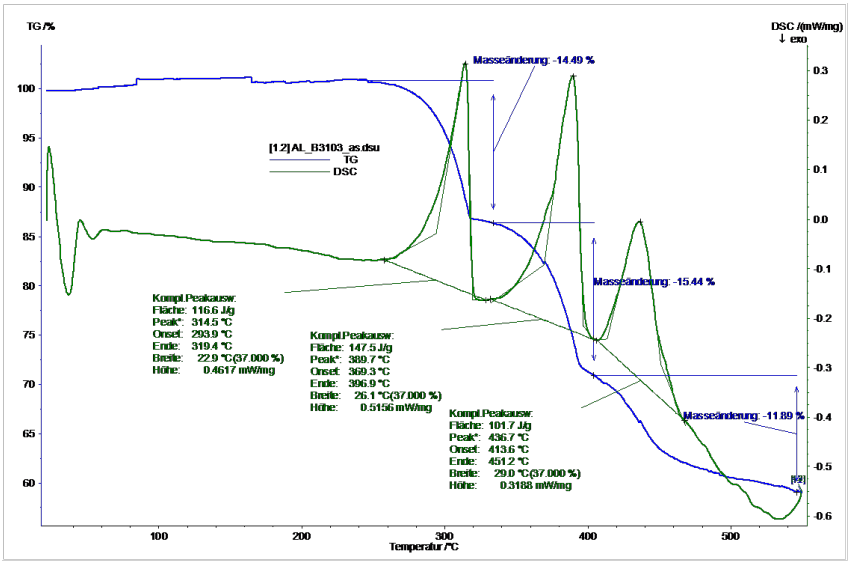

Figure 4.30: Thermogravimetric analysis of MIL-53*as*

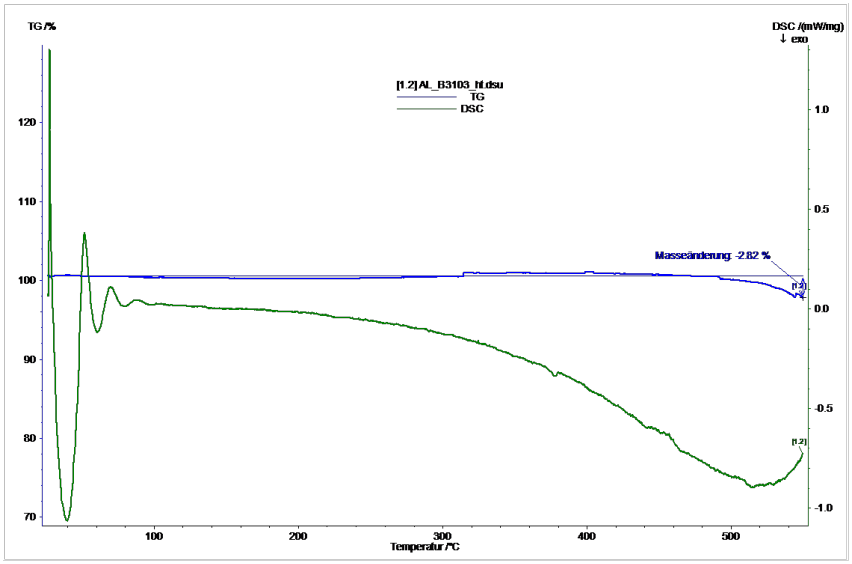

Figure 4.31: Thermogravimetric analysis of MIL-53*lt*

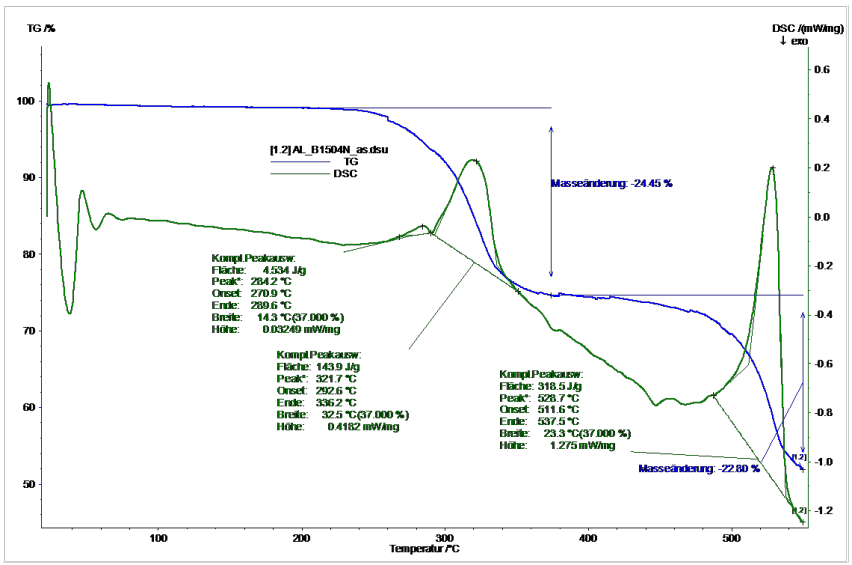

Figure 4.32: Thermogravimetric Analysis of MIL-53-NH_2*as*

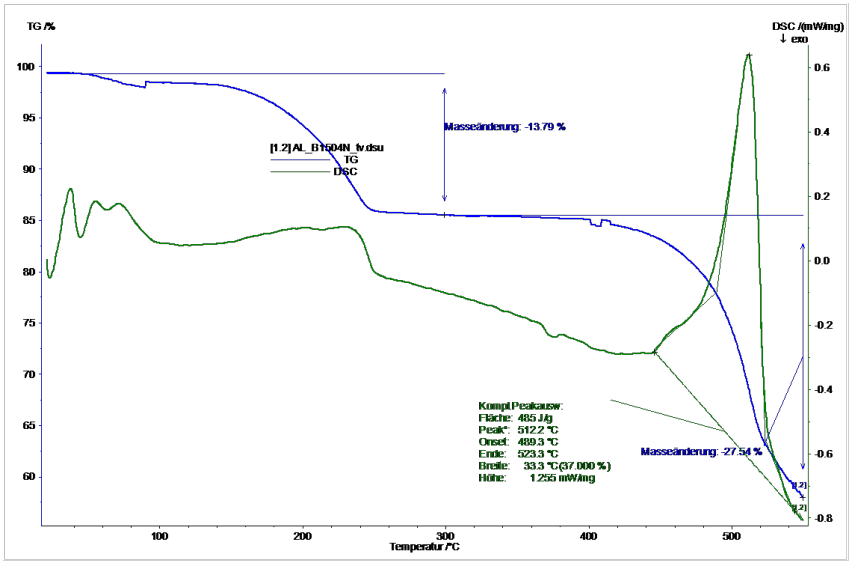

Figure 4.33: Themogravimetric analysis of MIL-53-NH_2*lt*

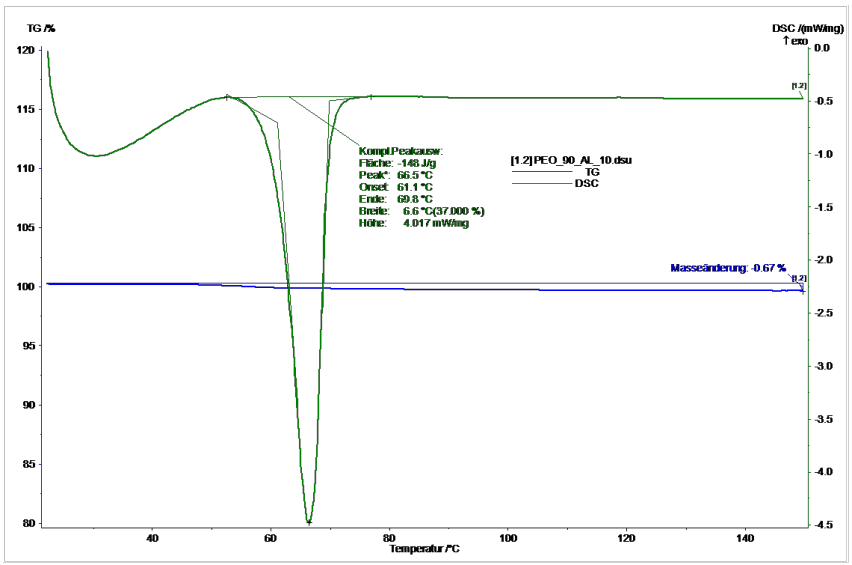

Figure 4.34: Themogravimetric analysis of a PEO membrane with 10 wt% MIL-53*lt*

Therefore, no strong influence of the MOF content on the melting point was observed. The impedance measurements of the membranes were performed up to 55 °C to avoid any phase transition of the membrane during the measurement.

4.2.3 Impedance measurements of the PEO membranes

Impedance measurements were performed in a range of −65 °C to 55 °C to avoid melting of the membranes. An example of the general nature of the results is shown in Figure 4.35 for a PEO membrane with $LiClO_4$ as conductive salt. The graphs for all other membranes measured are shown in the appendix.

It is notable in this figure, that the so-called DC plateau is only visible for temperatures as high as −35 °C and not for lower temperatures. The reason for this is, that the insulating properties of the membrane get more and more important at lower temperatures. Furthermore, the data points start to scatter a lot at low temperatures and low frequencies due to the low conductivity in that regime. This happens below $10^{-14}\,S\,cm^{-1}$ close to the limit of the detector. Therefore, only the conductivity at the DC plateau higher than −35 °C was used for creating an Arrhenius plot, Figure 4.36. The slope of the Arrhenius plot gives the activation energy E_a, indicated in the figure.

To compare the different membranes with each other, plots of the conductivities at the DC plateau at 50 °C and of the activation energy E_a including error bars are presented. First, membranes with no MIL-53*lt* and a content of 5 wt% and 10 wt% MIL-53*lt* are compared. The conductivities at 50 °C in Figure 4.37 show that the

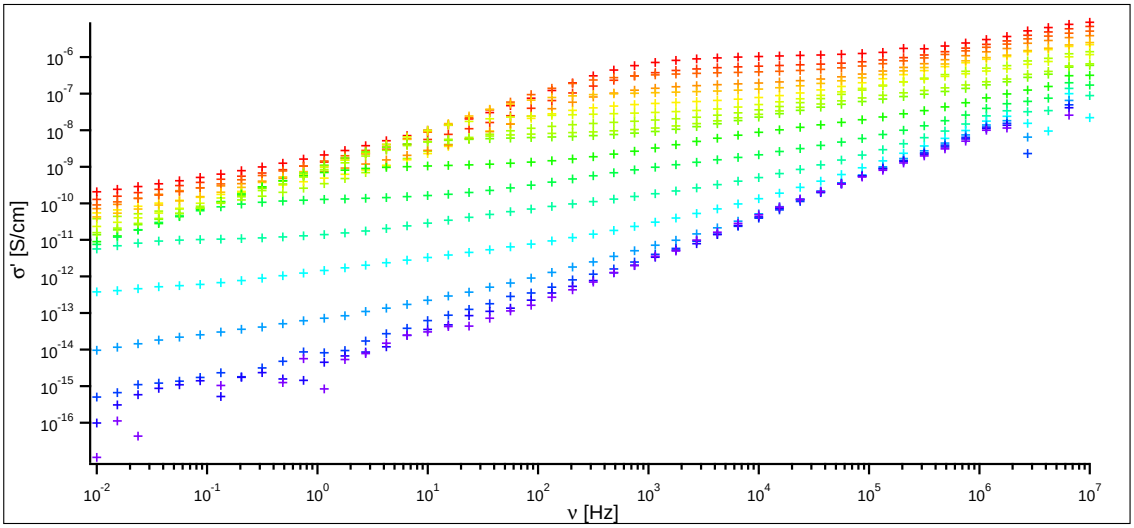

Figure 4.35: Impedance results for a PEO membrane with $LiClO_4$

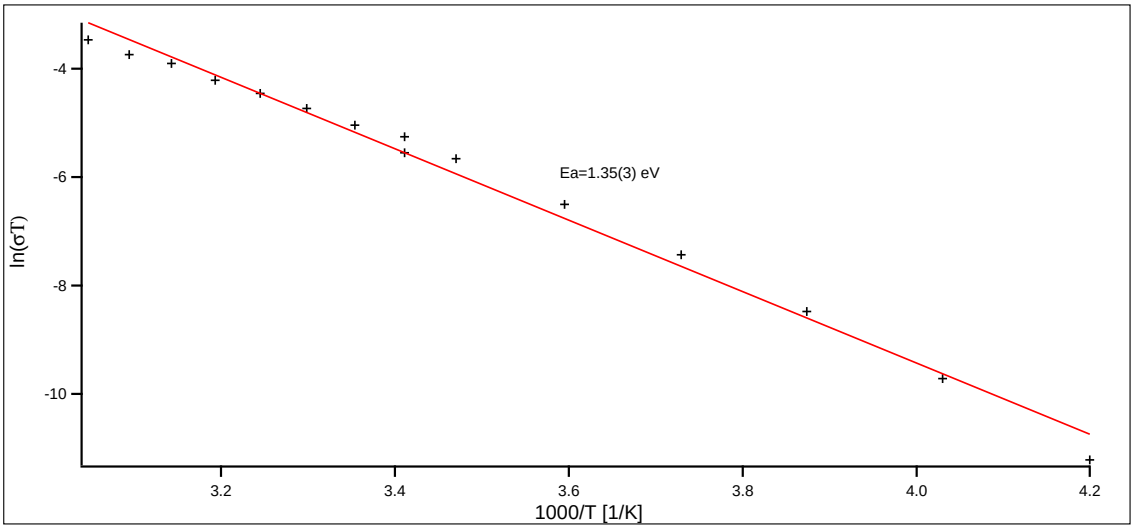

Figure 4.36: Arrhenius plot for a PEO membrane with $LiClO_4$

PEO membrane with no MIL-53*lt* is the most conductive one. The conductivity decreases with the increasing content of MIL-53*lt*. This pattern does not correspond to the activation energies for these membranes, shown in Figure 4.38. The activation energy of a membrane with 10 wt% is the lowest, followed by a plane PEO membrane and the membrane with 5 wt%. There may be other effects than only the content of MOF in the membrane. A plausible explanation could be air bubbles in the membrane which were unavoidable due to the casting technique or partly phase separation.

For the membranes with amine functionalized MIL-53-NH_2*lt* the conductivities vary as well, Figure 4.39. In this case the conductivity of the membrane with 5 wt% MIL-53-NH_2*lt* is the highest, followed by the membrane with no MIL-53-NH_2*lt* and 10 wt%. Here the conductivity at 50 °C increases with a small level of MOF and decreases drastically with the addition of more. Also the activation energies reassure this argument, Figure 4.40. The activation energy for the membrane with 5 wt% is the lowest, although the activation energies are within a narrow scale.

However, these results state quite clearly that the addition of MIL-53 derivatives to a PEO membrane do not necessarily enhance the lithium ion conductivity. Especially when measured below the melting point of the membrane, the additives can actually worsen the conductivity. In this work the prepared membranes were not measured above their melting point, because the characterization of the samples as solid state electrodes was the selected task. Additionally, the filler, MIL-53*lt* and MIL-53-NH_2*lt*, were ball milled before the casting to ensure a uniform distribution

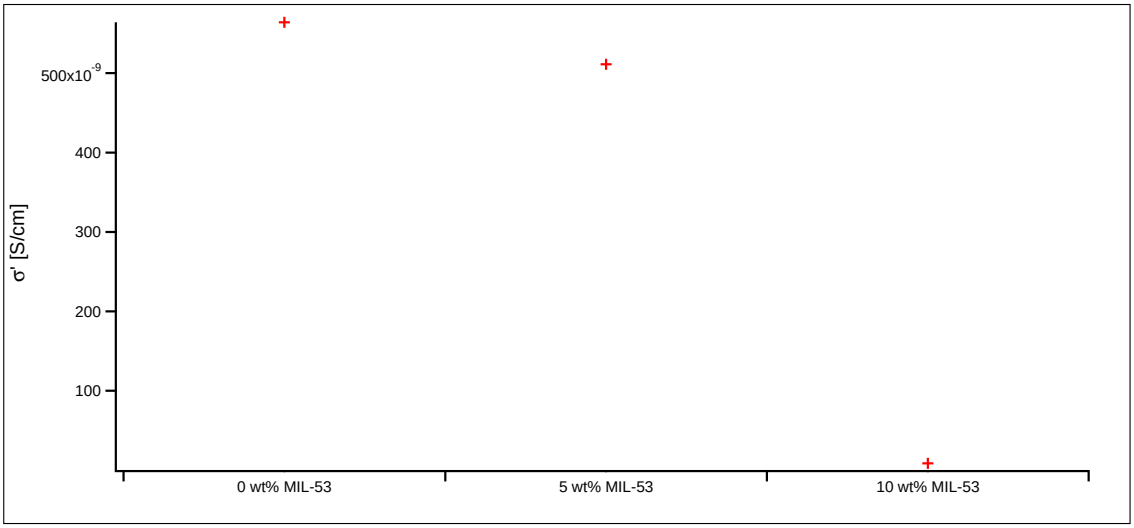

Figure 4.37: Impedance results for PEO membranes with varying content of MIL-53*lt* at 50 °C

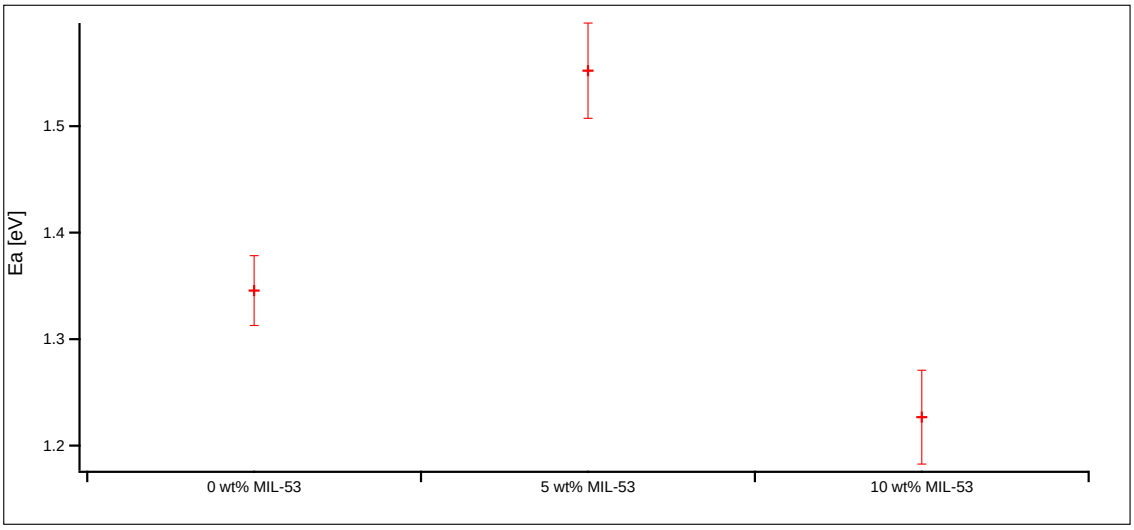

Figure 4.38: Comparison of activation energies for PEO membranes with varying content of MIL-53*lt*

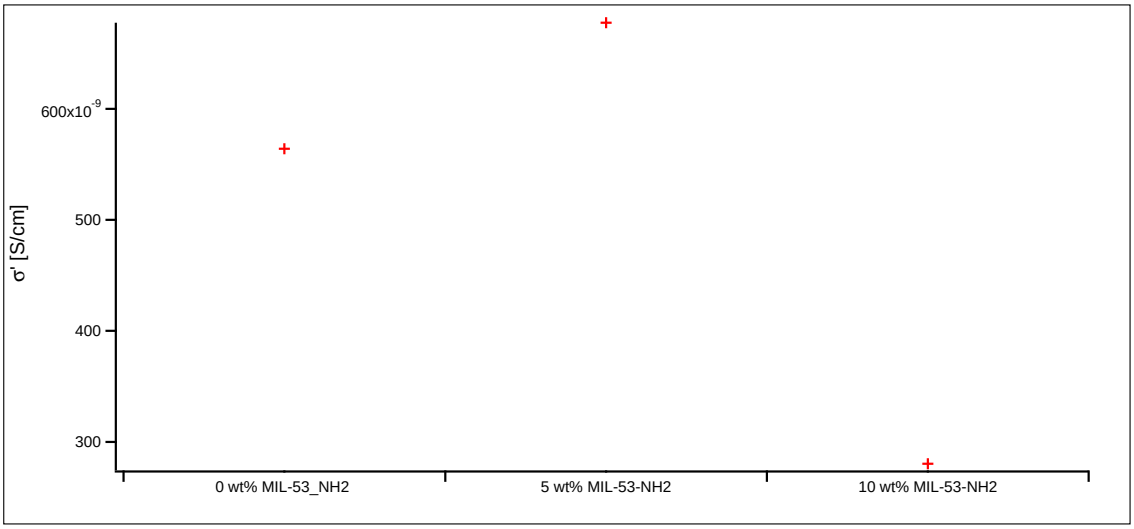

Figure 4.39: Impedance results for PEO membranes with varying content of MIL-53-NH_2*lt* at 50 °C

but no break up of the framework. Therefore, the MIL-53*lt* and MIL-53-NH_2*lt* were not nanometer-sized in the membrane.

It has been shown that fillers like nanometer-sized ceramic powders, Al_2O_3 or TiO_2, can enhance the conductivity of PEO membranes at room temperature. This effect can be observed due to the large surface area and Lewis acid character of the filler. It prevents the chain reorganization of the PEO membrane and therefore allows lithium ion transport not only at elevated temperatures but also at room temperature [17].

The pores of the metal organic framework in the as synthesized PEO membrane did not enhance the usable surface area, as would have been favoured. The pores seem to be too small to be entered by the PEO chains and if they are filled with lithium salt, they are not connected with each other to allow lithium transport.

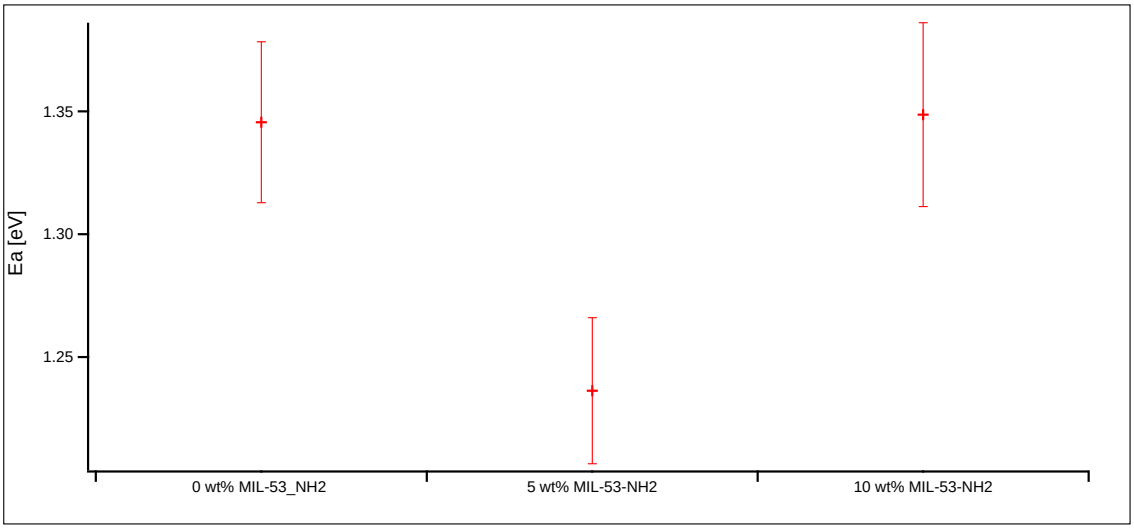

Figure 4.40: Comparison of activation energies for PEO membranes with varying content of MIL-53-NH_2*lt*

5 Conclusion

The synthesis of UiO-66 and UiO-66-NH_2 is already well known and is therefore already optimized in the lab scale. It was no problem to synthesize these products and confirm their structure and chemical composition with powder X-ray diffraction and ATR-IR measurements. Also the thermogravimetric properties correspond to data known. The grafting with different alkoxides under inert atmosphere produced a material with lithium ions in the structure which can participate in lithium ion conductivity. The grafted samples were not stable up to high temperatures due to the loss of the alkoxide from the structure. Therefore the samples were measured up to 65 °C. With a T_1 analysis by NMR, short range movement of lithium ions in the structure was observed. Using impedance spectroscopy measurements, all different samples were investigated for their lithium ion conductivity. Pellets soaked with a maximum amount of propylene carbonate were used to measure these ionic conductivities.

The results indicate that different blends of UiO-66 or UiO-66-NH_2 and one of the alkoxide derivatives show a wide variety of conductivity and also different activation energies. Therefore also the steric constraints may play a big role in the strength of the bonding of the lithium ion in the structure. These effects may need more research, especially the structure clarification of the grafted samples that are not known until now.

Measurements of the same samples under pressure revealed an increase of conductivity at room temperature to some extent. The increase can be explained with a better contact between the soaked pellet and the electrodes.

The Al-based MOF, MIL-53-(Al) and MIL-53-NH_2(Al), were adapted for the creation of PEO membranes including a conductive lithium salt. These membranes were optimized to avoid phase separation and recrystallisation of the salt after removal of the solvent. The membranes containing MIL-53(Al) or MIL-53-NH_2(Al) do not show any improvement or decline in the thermal properties. They do show a decline of the conductivity according to the content of Al-based MOF in the membrane if measured in the solid regime. These membranes were not measured at higher temperatures than their melting point.

Bibliography

[1] Kuppler, R. J., Timmons, D. J., Fang, Q.-R., Li, J.-R., Makal, T. A., Young, M. D., Yuan, D., Zhao, D., Zhuang, W., and Zhou, H.-C. *Coordination Chemsitry Reviews* (253), 3042–3066 (2009).

[2] Ke, F.-S., Wu, Y.-S., and Deng, H. *Journal of Solid State Chemistry* **223**, 109–121 (2015).

[3] Saravanan, K., Nagarathinam, M., Balaya, P., and Vittal, J. J. *Journal of Materials Chemistry* (20), 8329–8335 (2010).

[4] Wiers, B. M., Foo, M.-L., Balsara, N. P., and Long, J. R. *J. Am. Chem. Soc.* **133**, 14522–14525 (2011).

[5] Piscopo, C. G., Polyzoidis, A., Schwarzer, M., and Loebbecke, S. *Microporous and Mesoporous Materials* **208**, 30–35 (2015).

[6] Schaate, A., Roy, P., Godt, A., Lippke, J., Waltz, F., Wiebcke, M., and Behrens, P. *Chem. Eur. J.* **17**, 6643–6651 (2011).

[7] Katz, M. J., Brown, Z. J., Colon, Y. J., Siu, P. W., Scheidt, K. A., Snurr, R. Q., Hupp, J. T., and K., F. O. *Chem. Commun.* **49**, 9449–9451 (2013).

[8] Ameloot, R., Aubrey, M., Wiers, B. M., Gomora-Figueroa, A. P., Patel, A. N., Balsara, N. P., and Long, J. R. *Chem. Eur. J.* **19**, 5533–5536 (2013).

[9] Ahnfeldt, T., Gunzelmann, D., Loiseau, T., Hirsemann, D., Senker, J., Ferey, G., and Stock, N. *Inorganic Chemistry* **48**(7), 3057–3064 (2009).

[10] Loiseau, T., Serre, C., Huguenard, C., Fink, G., Taulelle, F., Henry, M., Bataille, T., and Ferey, G. *Chem. Eur. J.* **10**, 1373–1382 (2004).

[11] Qian, X., Yadian, B., Wu, R., Long, Y., Zhou, K., Zhu, B., and Huang, Y. *International Journal of Hydrogen Energy* **38**, 16710–16715 (2013).

[12] Morrison, R. C., Kamienski, C. W., and Schwindeman, J. A. (Dec. 10, 1996).

[13] Larkin, P. *Infrared and raman spectroscopy: principels and spectral interpretation.* Elsevier, 1. edition, (2011).

[14] Barsoukov, E. and Macdonald, J. R., editors. *Impedance Spectroscopy: Theory, Experiment, and Applications.* John Wiley & Sons, Inc., Hoboken, New Jersey, 2. edition, (2005).

[15] Ershow, M., Liu, H. C., Li, L., Buchanan, M., Wasilewski, Z. R., and Jonscher, A. K. *IEEE Transactions on Electron Devices* **45**(10) (1998).

[16] Khan, A. I., Chatterjee, K., Wang, B., Drapcho, S., You, L., Serrao, C., Bakaul, S. R., R., R., and Salahuddin, S. *Nature Materials* **14**, 182–186 (2015).

[17] Croce, F., Appetecchi, G. B., Persi, L., and Scrosati, B. *Nature* **394**, 456–458 (1998).

[18] Finsy, V., Ma, L., Alaerts, L., De Vos, D. E., Baron, G. V., and Denayer, J. F. M. *Microporous and Mesoporous Materials* **120**, 221–227 (2009).

[19] Himsl, D., Wallacher, D., and Hartmann, M. *Angew. Chem. Int. Ed.* **48**, 4639–4642 (2009).

[20] Klontzas, E., Mavrandonakis, A., Tylianakis, E., and Froudakis, G. E. *Nano Letters* **8**(6), 1572–1576 (2008).

[21] Lemaitre-Auger, F. and Prud'homme, J. *Electrochimica Acta* **46**, 1359–1367 (2001).

[22] Lochmann, L. *Eur. J. Inorg. Chem.* , 1115–1126 (2000).

[23] Marzantowicz, M., Dygas, J. R., and Krok, F. *Electrochimica Acta* **53**, 7417–7425 (2008).

[24] Mosa, J., Aparicio, M., Tadanaga, K., Hayashi, A., and Tatsumisago, M. *Electrochimica Acta* **149**, 293–299 (2014).

[25] Mulfort, K. L., Farha, O. K., Stern, C. L., Sarjeant, A. A., and Hupp, J. T. *J. Am. Chem. Soc.* **131**(11), 3866–3868 (2009).

[26] Serraino Fiory, F., Croce, F., D'Epifanio, A., Licoccia, S., Scrosati, B., and Traversa, E. *Journal of the European Ceramic Society* **24**, 1385–1387 (2004).

[27] Zhang, S. S. *Journal of The Electrochemical Society* **160**(9), A1421–A1424 (2013).

List of abbrevations

as as synthesized modification

ATR-IR Attenuated total reflection infra-red spectroscopy

ht high temperature modification

Li-2m2p Lithium 2-methyl-2-pentoxide

Li-3m3p Lithium 3-methyl-3-pentoxide

LitBu Lithium tertiary-butoxide

Li-TEG Lithium tetra ethylene glycol

lt low temperature modification

MIL Materials from Institut Lavoisier

MOF Metal Organic Framework

PEO Polyethylene oxide

PSM Post synthetic modification

SBU Secondary building unit

UiO Universitetet i Oslo

A Appendix

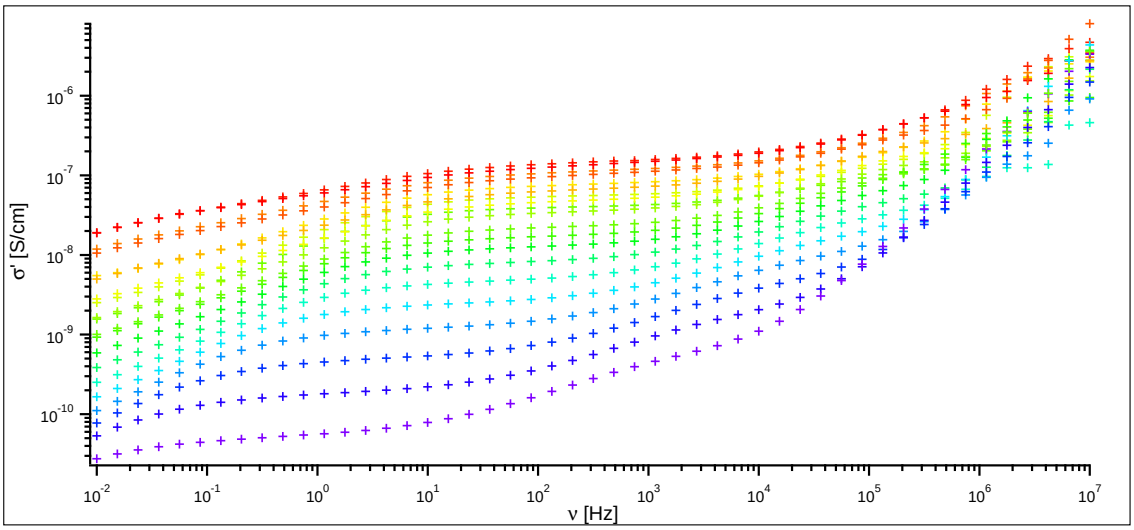

Figure A.1: Impedance results for UiO-66 grafted with lithium tertiary-butoxide

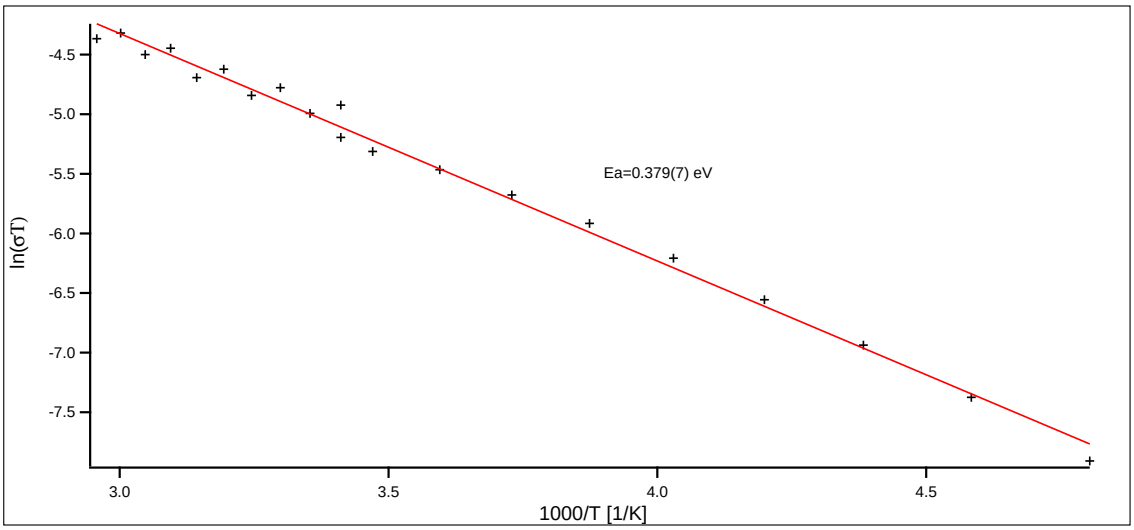

Figure A.2: Arrhenius plot for UiO-66 grafted with lithium tertiary-butoxide

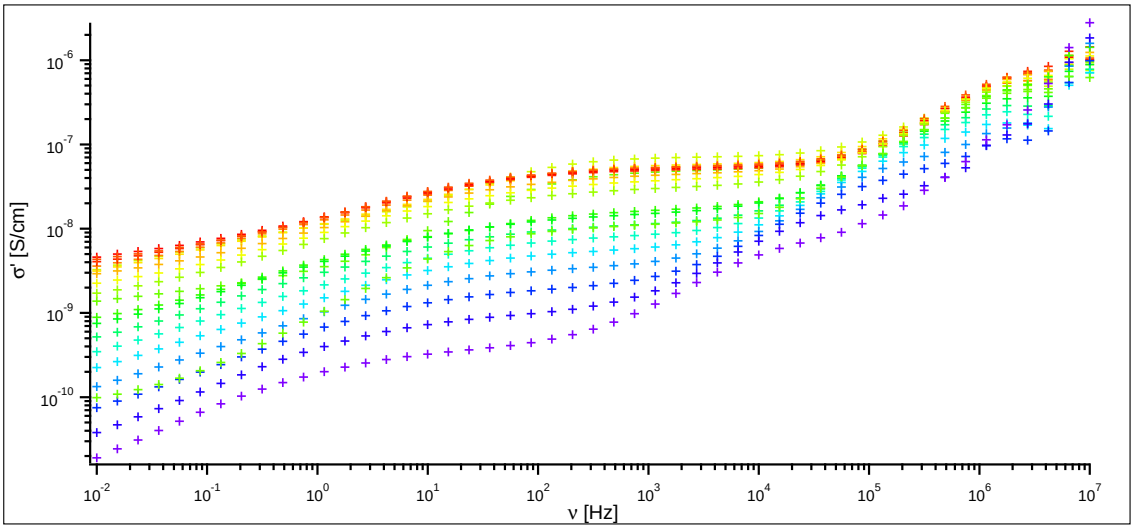

Figure A.3: Impedance results for UiO-66 grafted with lithium 2-methyl-2-pentoxide

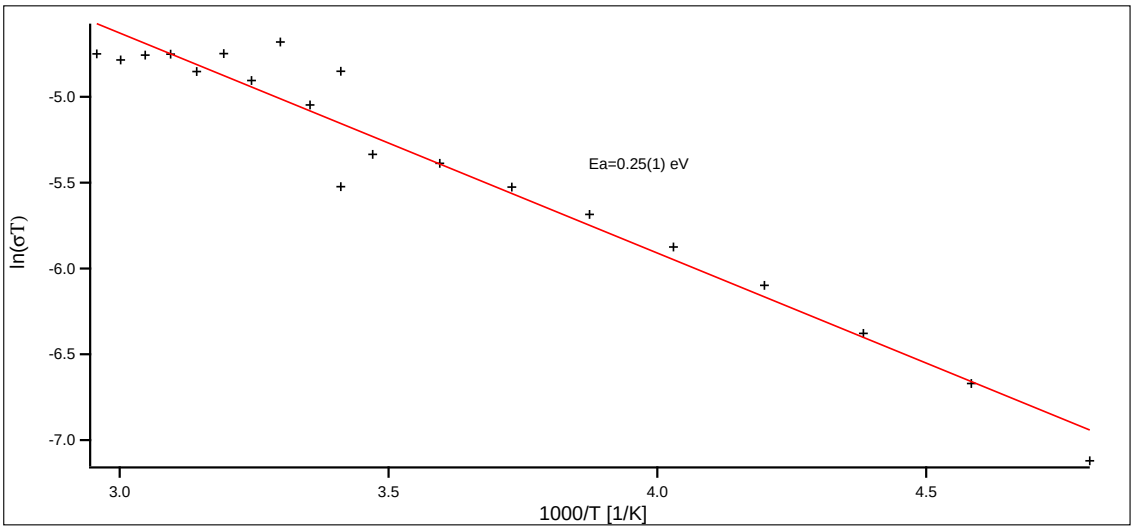

Figure A.4: Arrhenius plotfor UiO-66 grafted with lithium 2-methyl-2-pentoxide

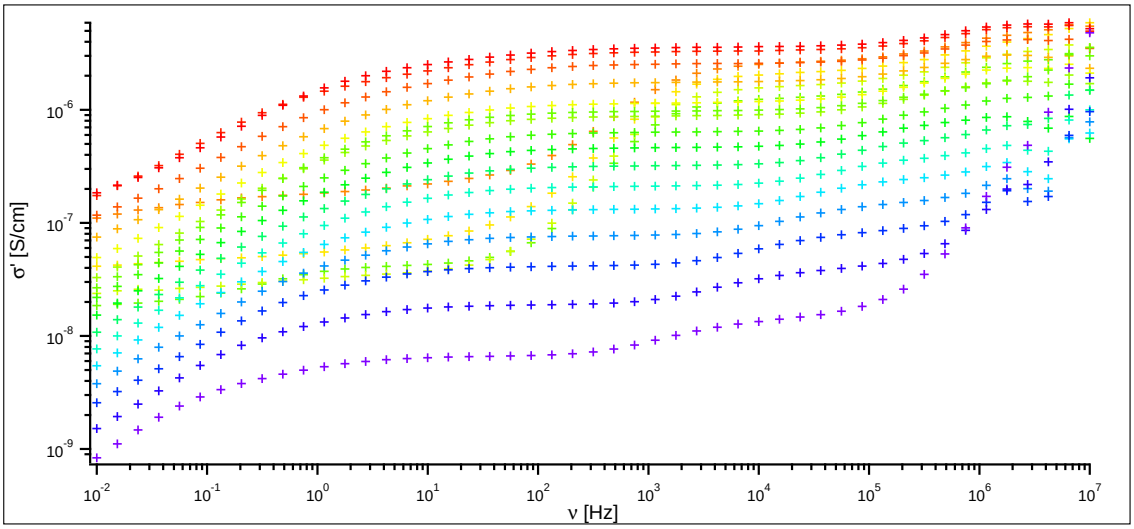

Figure A.5: Impedance results for UiO-66 grafted with lithium 3-methyl-3-pentoxide

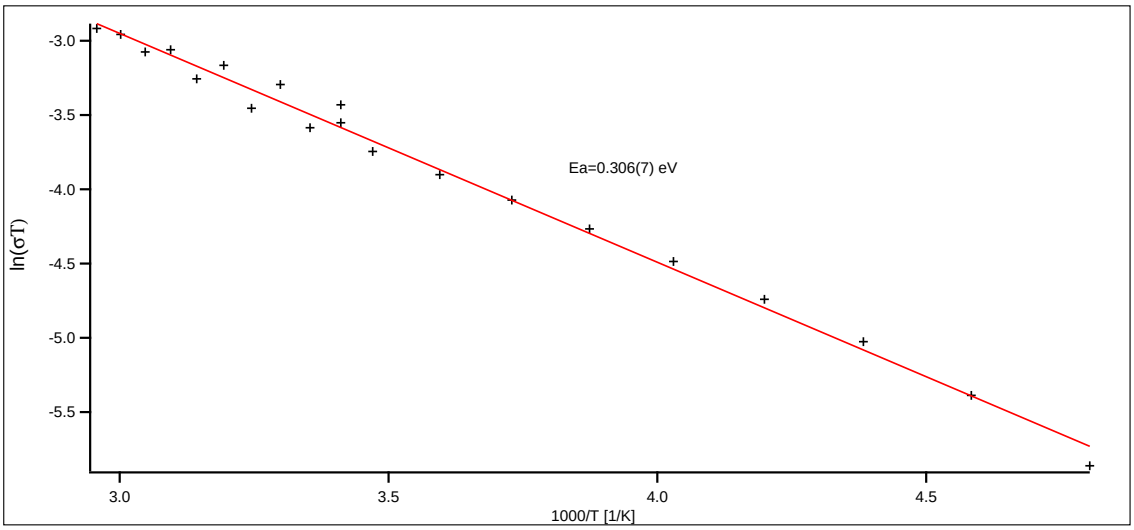

Figure A.6: Arrhenius plot for UiO-66 grafted with lithium 3-methyl-3-pentoxide

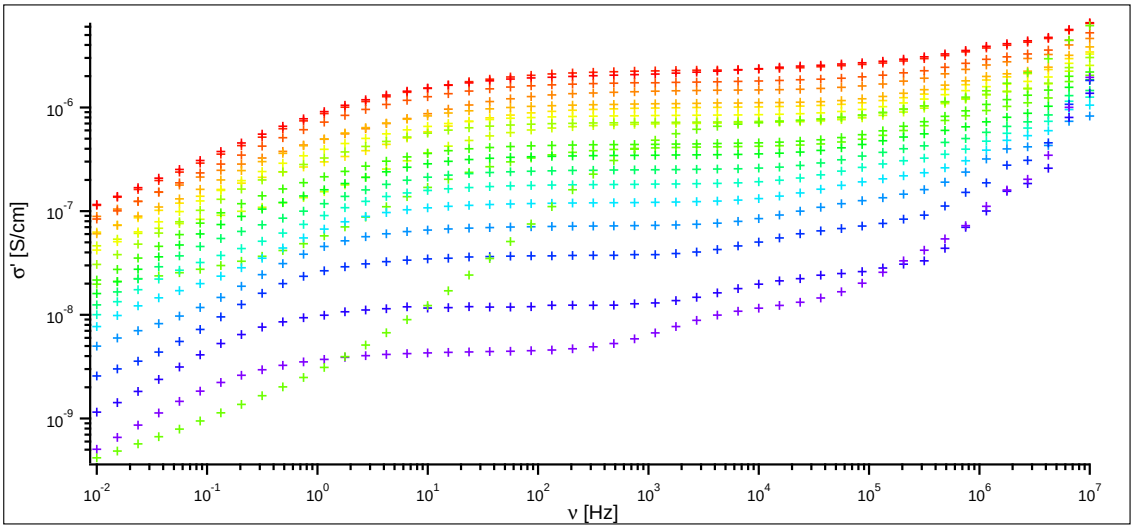

Figure A.7: Impedance results for UiO-66 grafted with lithium 3-methyl-3-pentoxide with grease

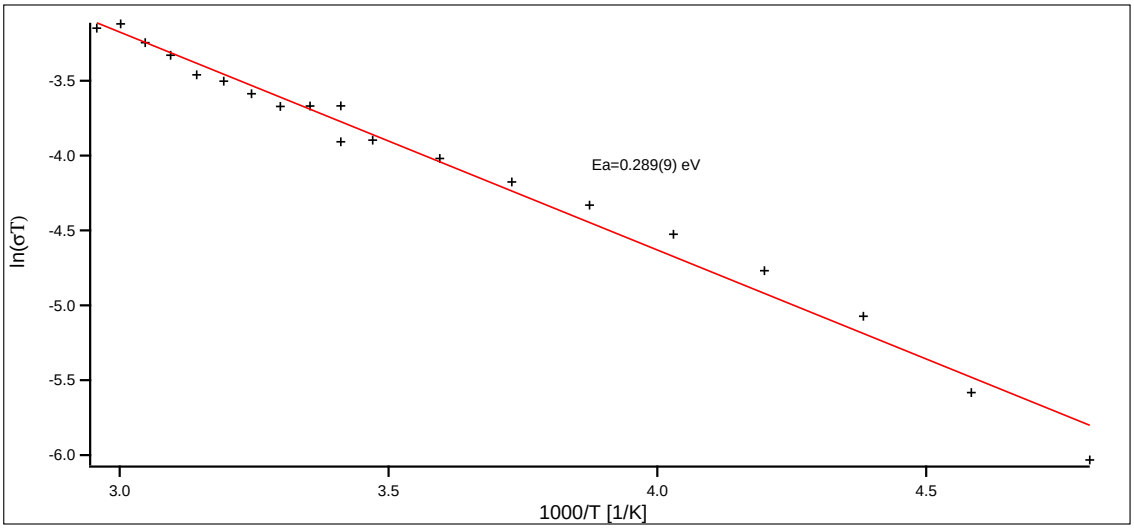

Figure A.8: Arrhenius plot for UiO-66 grafted with lithium 3-methyl-3-pentoxide with grease

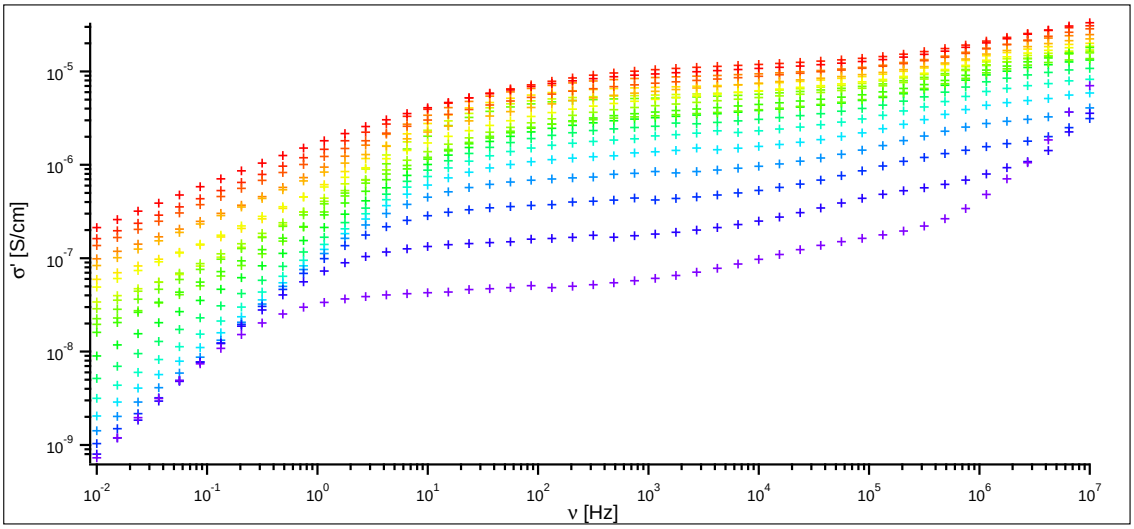

Figure A.9: Impedance results for UiO-66 grafted with lithium tetraethylene glycol

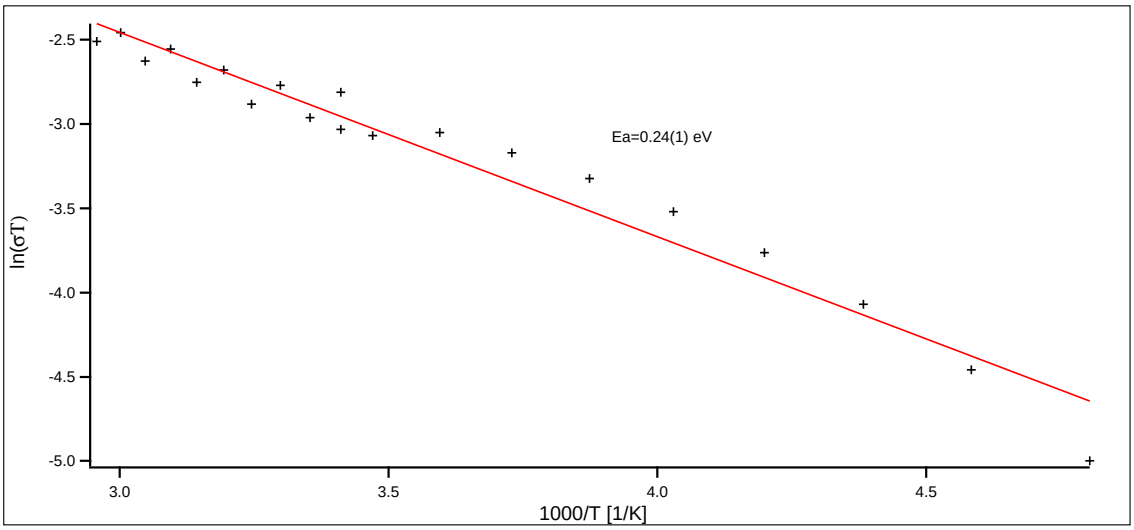

Figure A.10: Arrhenius plot for UiO-66 grafted with lithium tetraethylene glycol

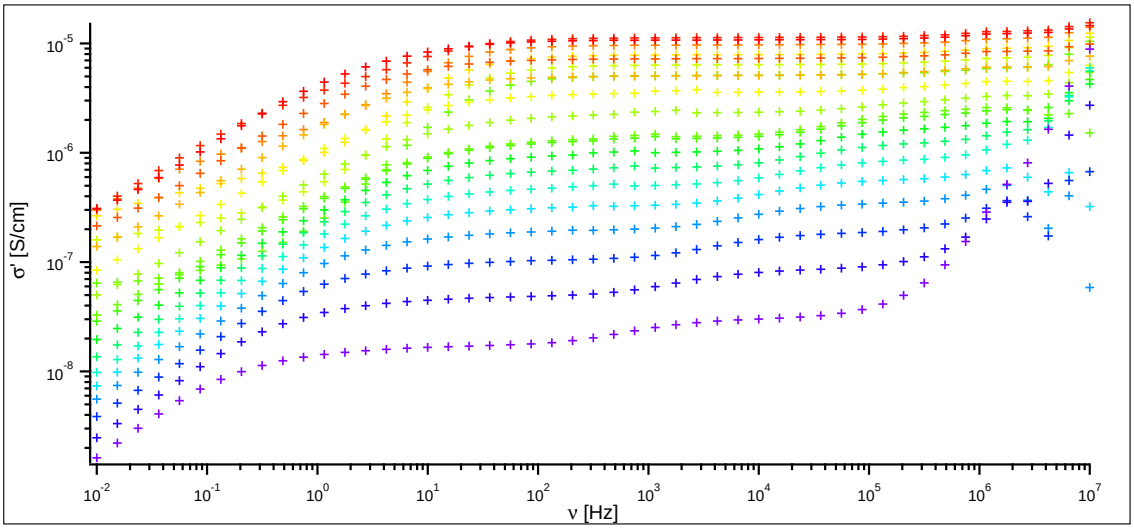

Figure A.11: Impedance results for UiO-66-NH_2 grafted with lithium tertiary-butoxide

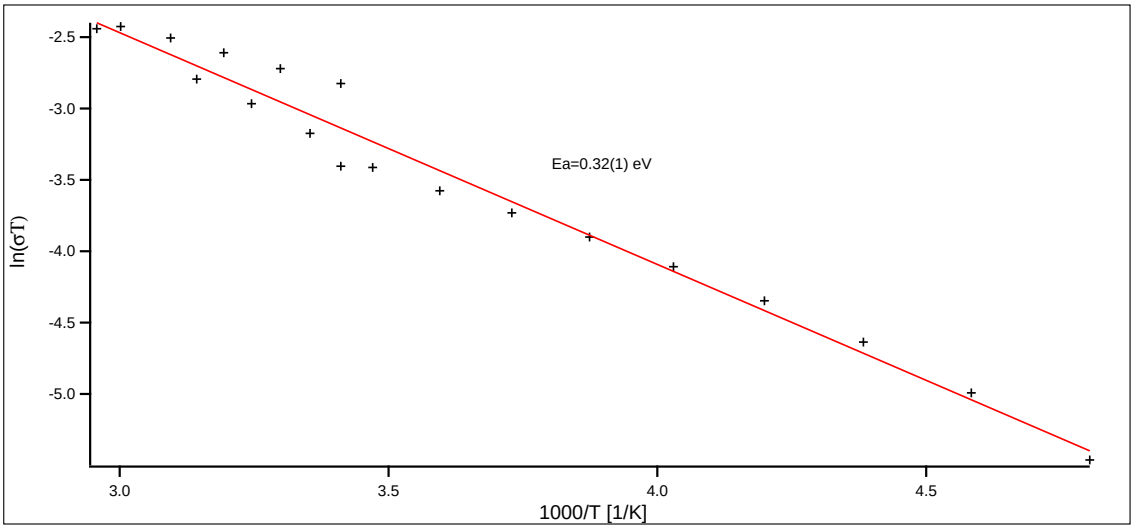

Figure A.12: Arrhenius plot for UiO-66-NH_2 grafted with lithium tertiary-butoxide

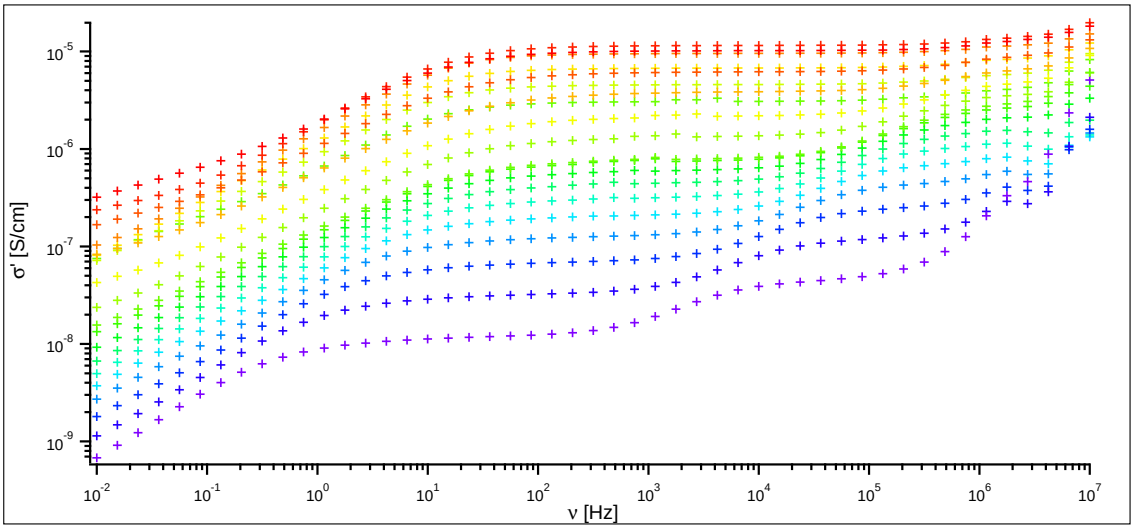

Figure A.13: Impedance results for UiO-66-NH_2 grafted with lithium 2-methyl-2-pentoxide

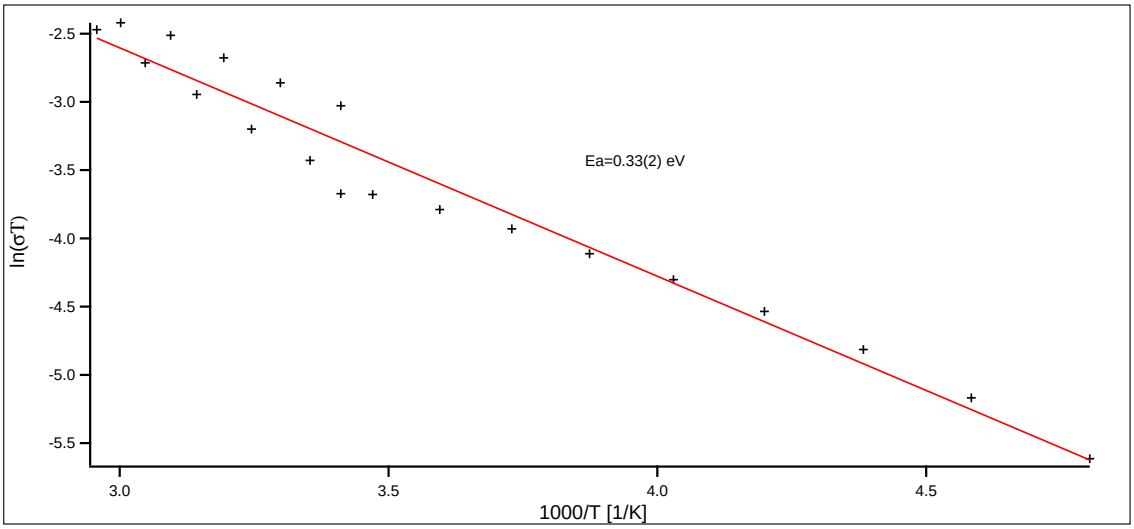

Figure A.14: Arrhenius plotfor UiO-66-NH_2 grafted with lithium 2-methyl-2-pentoxide

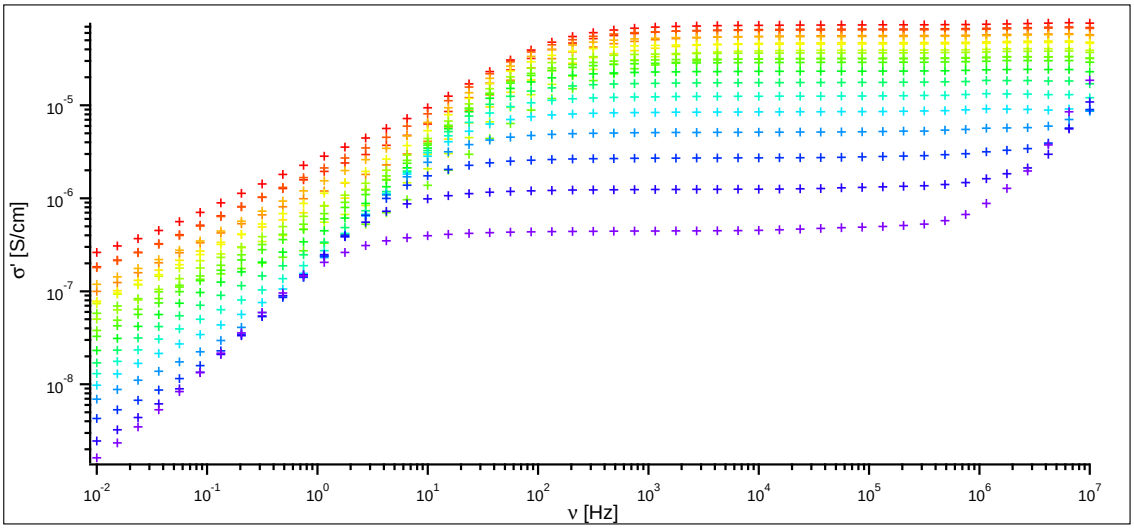

Figure A.15: Impedance results for UiO-66-NH_2 grafted with lithium 3-methyl-3-pentoxide

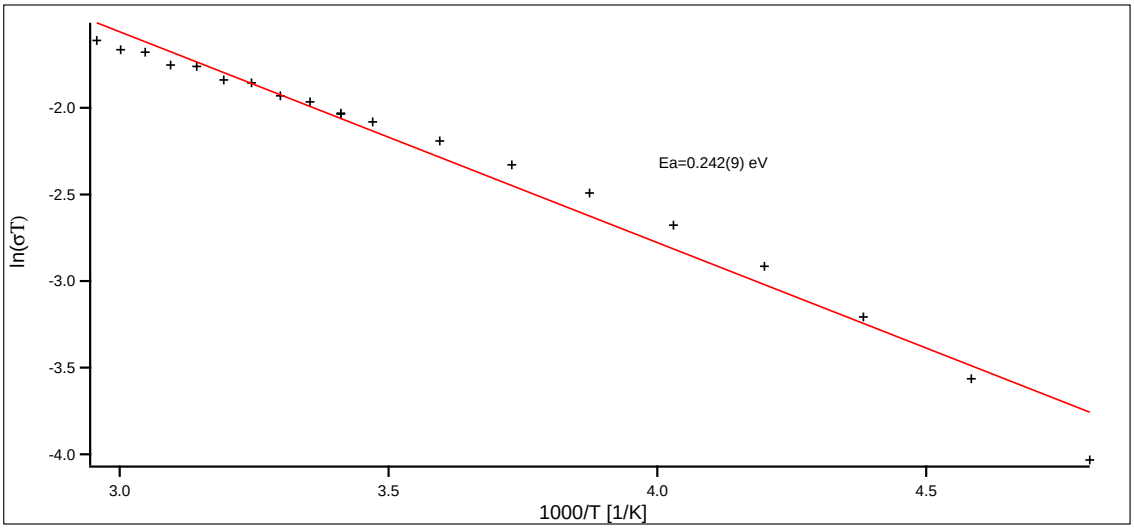

Figure A.16: Arrhenius plot for UiO-66-NH_2 grafted with lithium 3-methyl-3-pentoxide

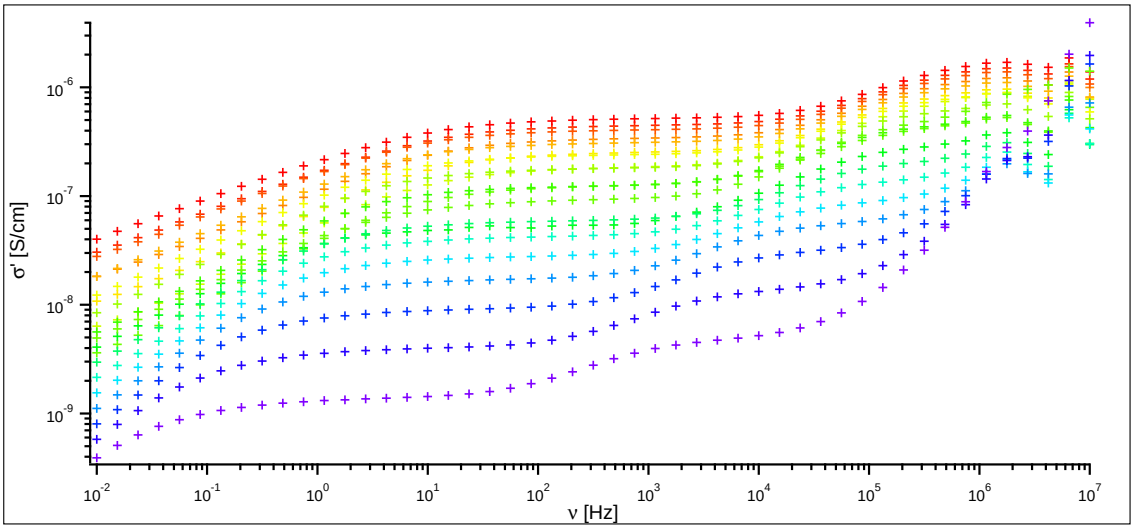

Figure A.17: Impedance results for UiO-66-NH_2 grafted with lithium 3-methyl-3-pentoxide with grease

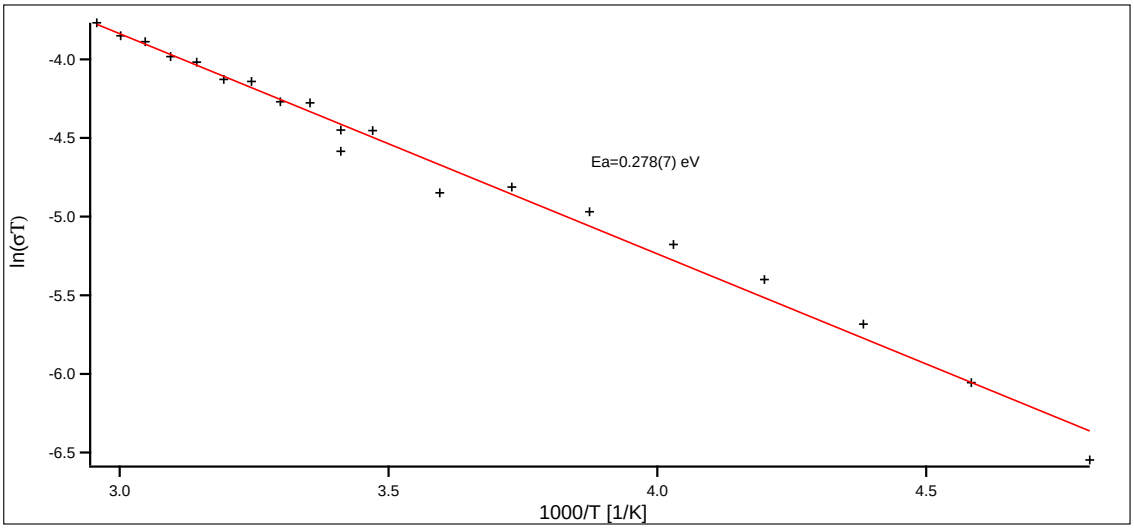

Figure A.18: Arrhenius plot for UiO-66-NH_2 grafted with lithium 3-methyl-3-pentoxide with grease

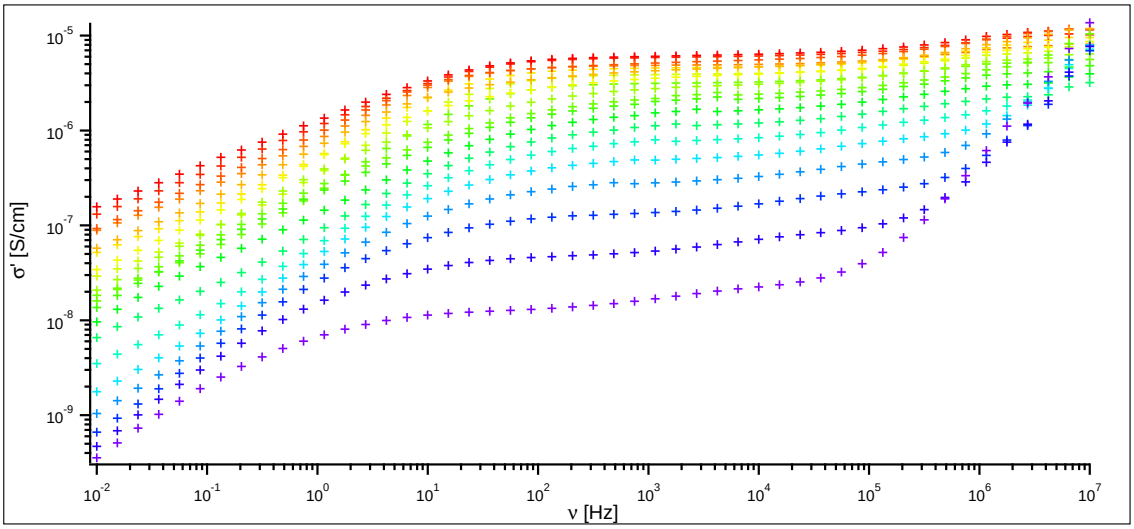

Figure A.19: Impedance results for UiO-66-NH_2 grafted with lithium tetraethylene glycol

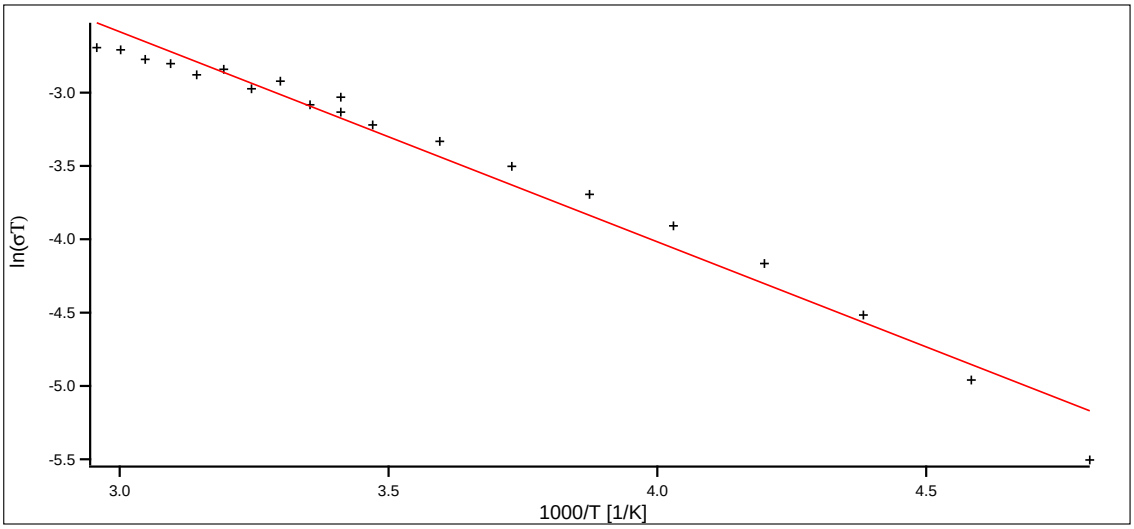

Figure A.20: Arrhenius plot for UiO-66-NH_2 grafted with lithium tetraethylene glycol

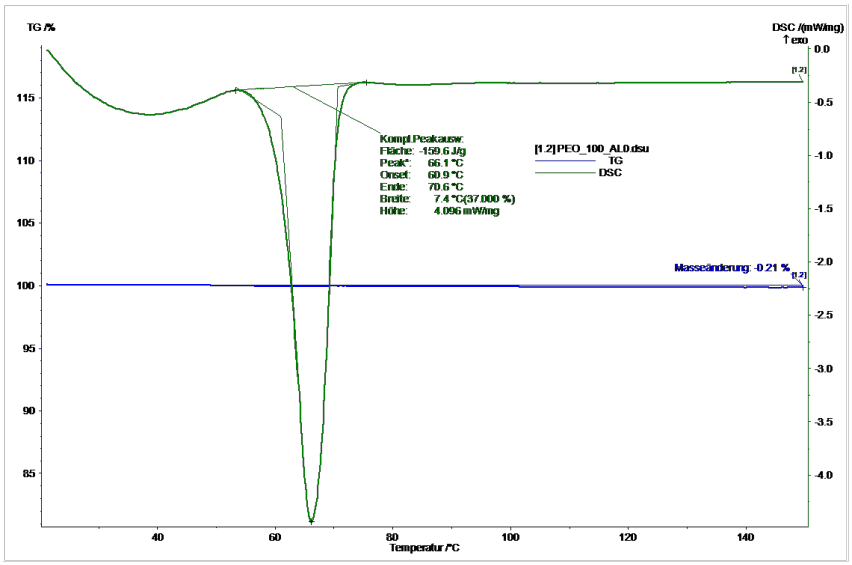

Figure A.21: Themogravimetric analysis of the PEO membrane with 0 wt% MIL-53(Al)

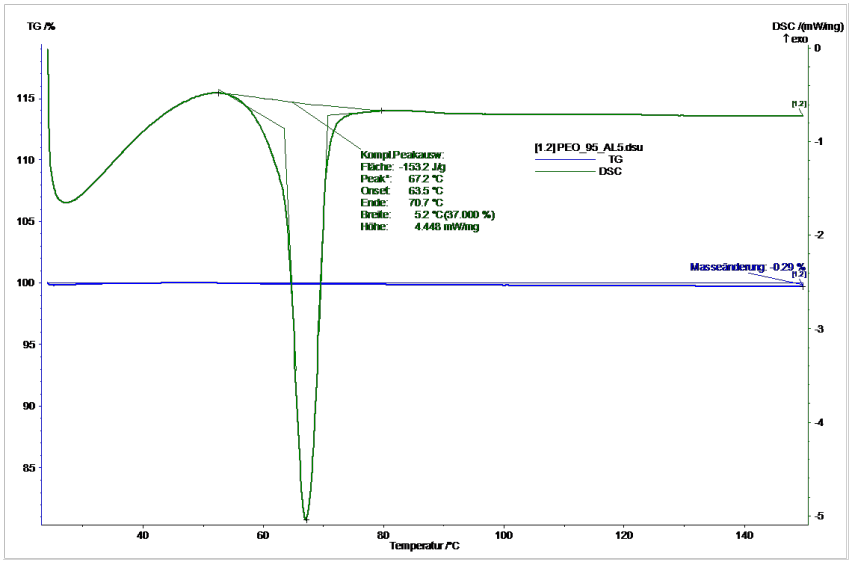

Figure A.22: Themogravimetric analysis of the PEO membrane with 5 wt% MIL-53(Al)

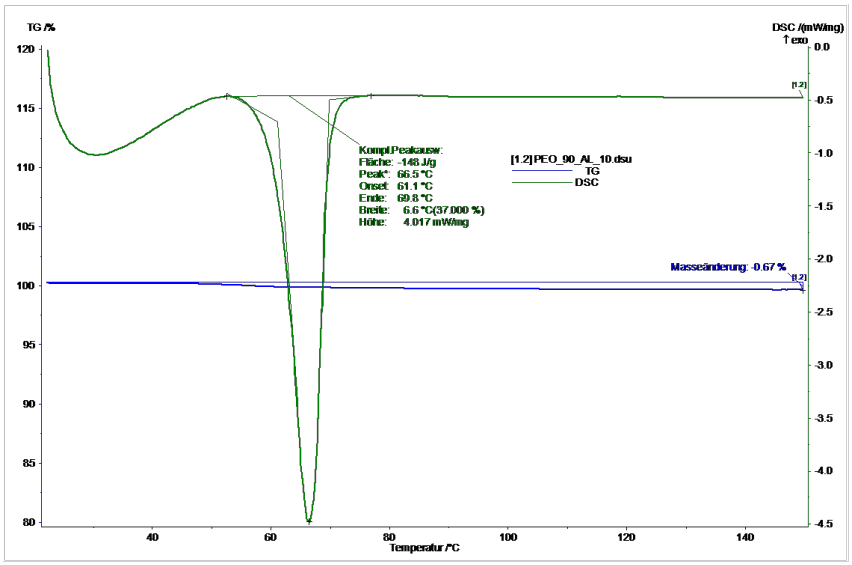

Figure A.23: Themogravimetric analysis of the PEO membrane with 10 wt% MIL-53(Al)

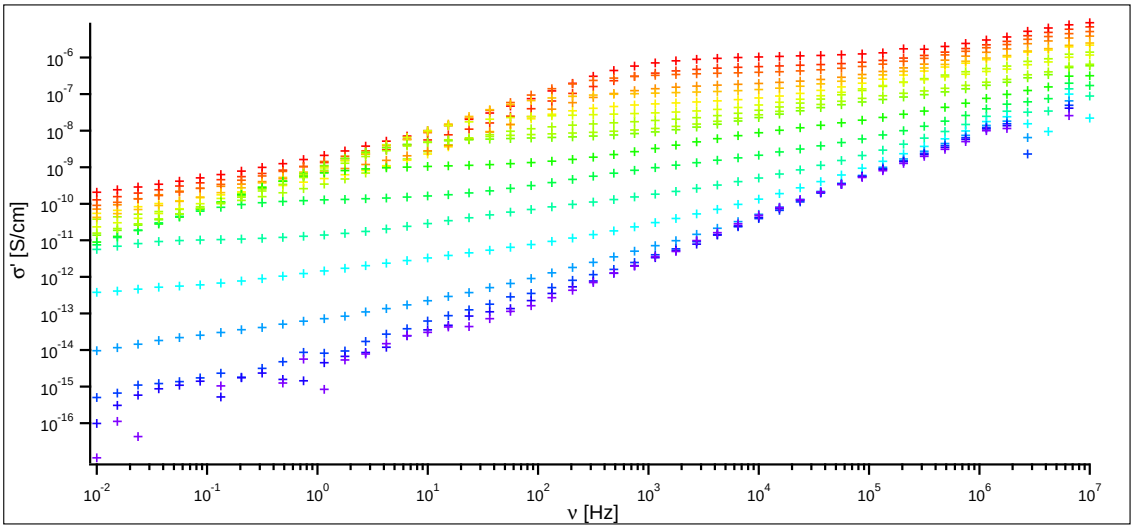

Figure A.24: Impedance results for the PEO membrane with 0 wt% MIL-53(Al)

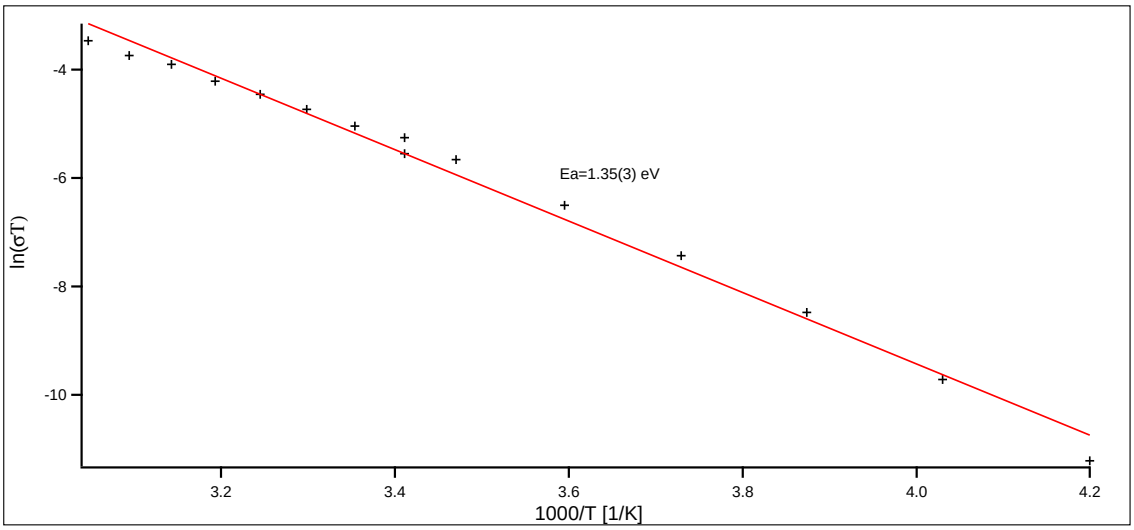

Figure A.25: Arrhenius plot for the PEO membrane with 0 wt% MIL-53(Al)

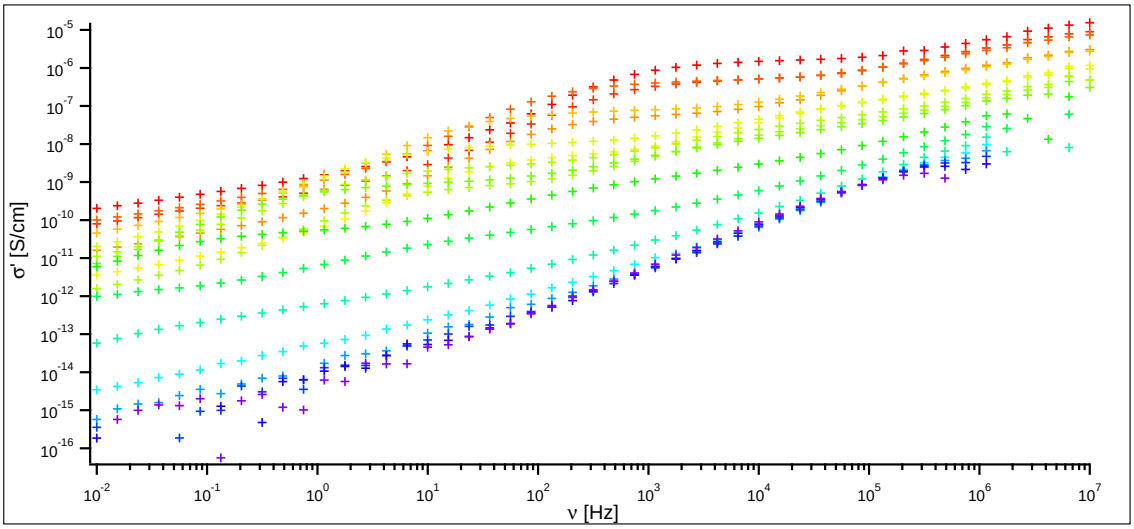

Figure A.26: Impedance results for the PEO membrane with 5 wt% MIL-53(Al)

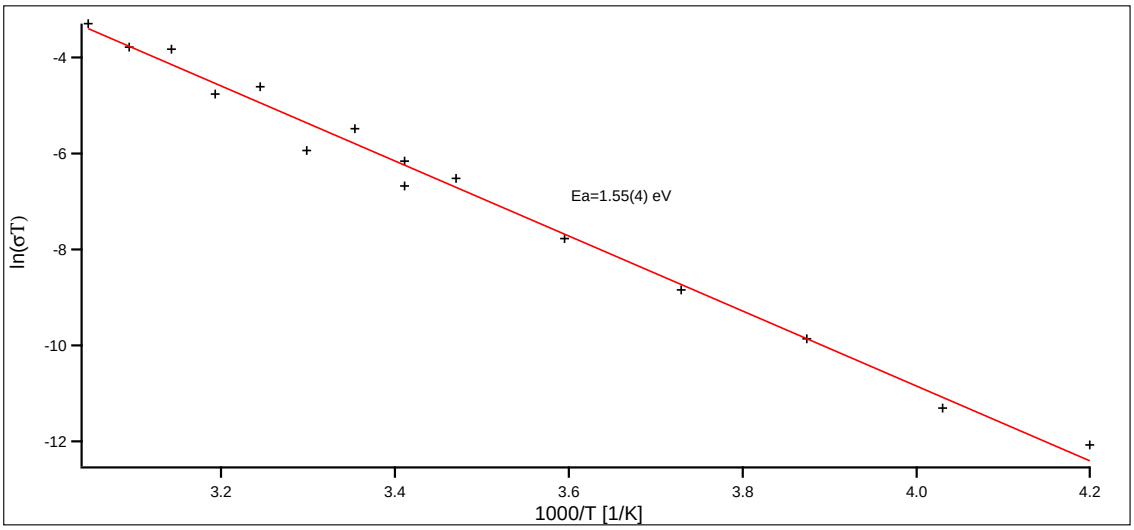

Figure A.27: Arrhenius plot for the PEO membrane with 5 wt% MIL-53(Al)

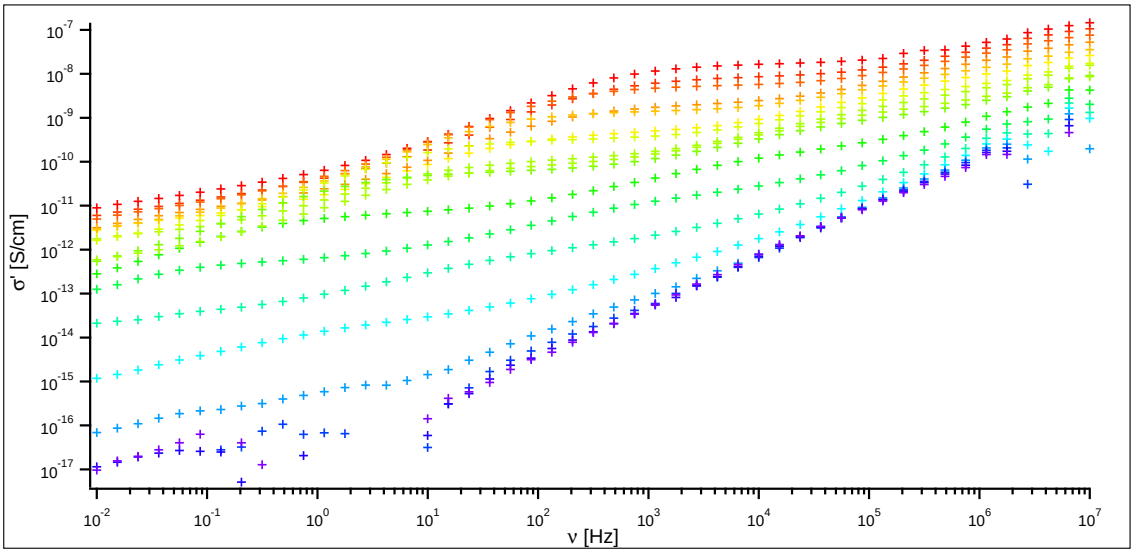

Figure A.28: Impedance results for the PEO membrane with 10 wt% MIL-53(Al)

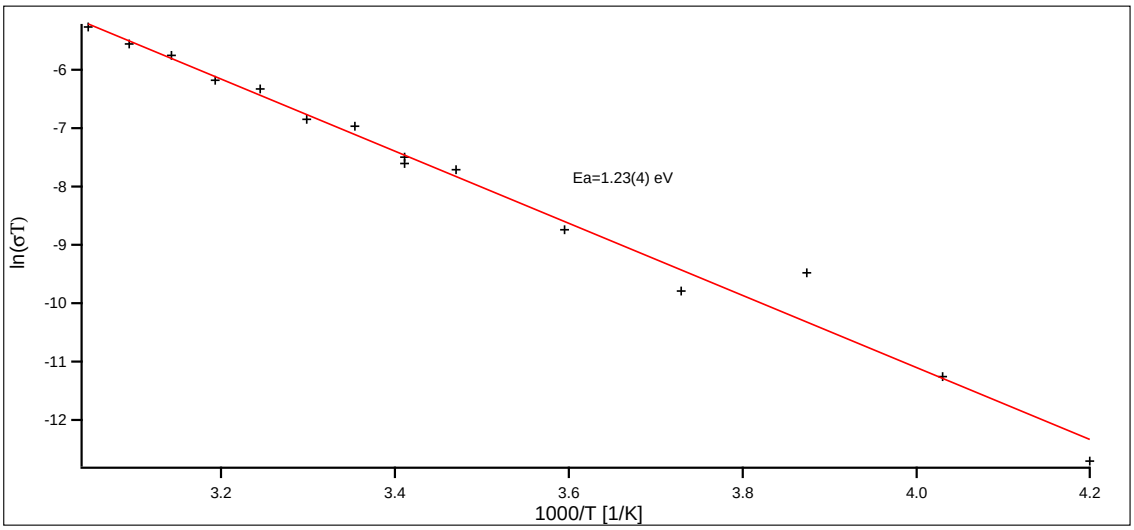

Figure A.29: Arrhenius plot for the PEO membrane with 10 wt% MIL-53(Al)

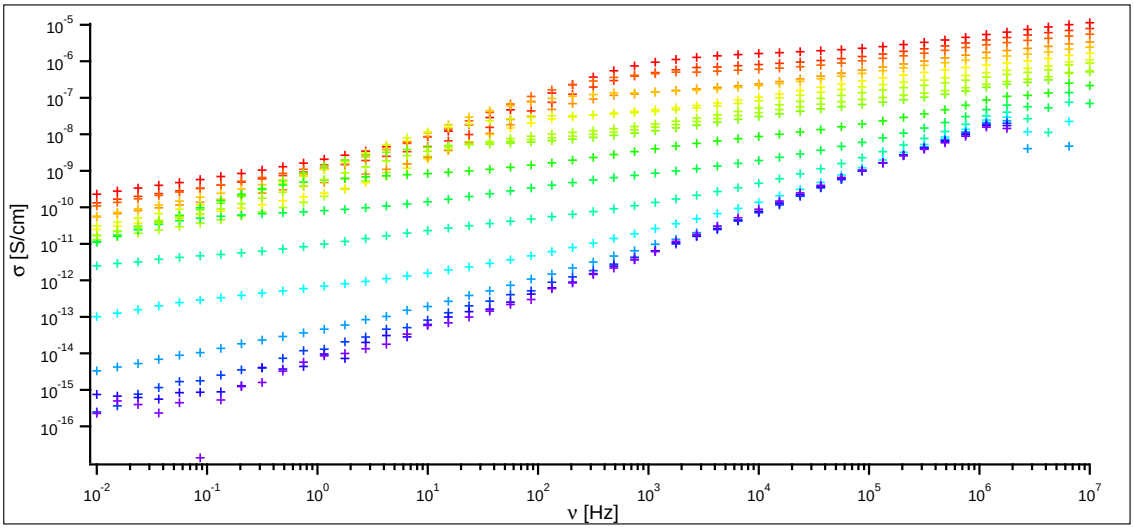

Figure A.30: Impedance results for the PEO membrane with 5 wt% MIL-53-NH_2(Al)

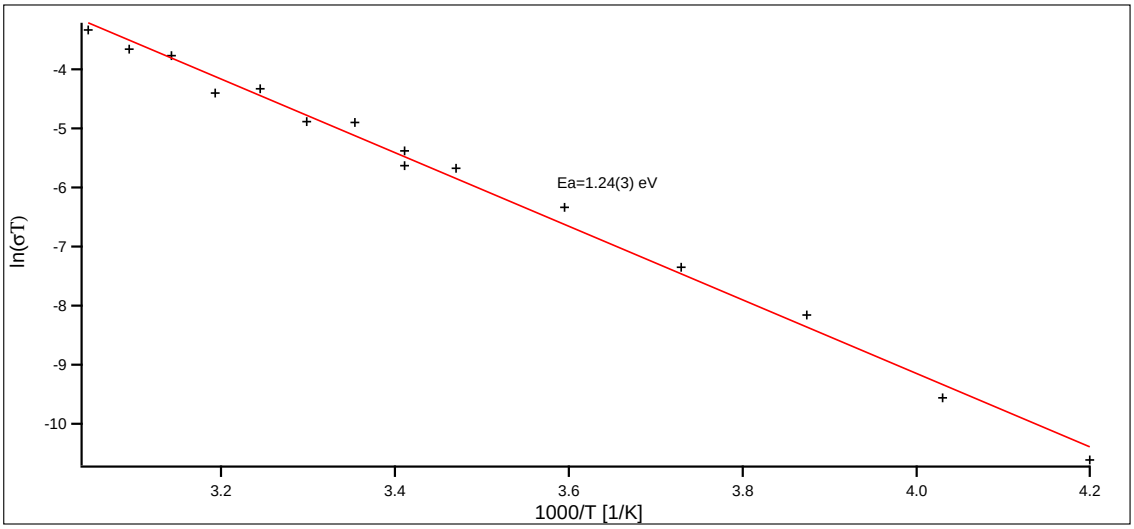

Figure A.31: Arrhenius plot for the PEO membrane with 5 wt% MIL-53NH_2(Al)

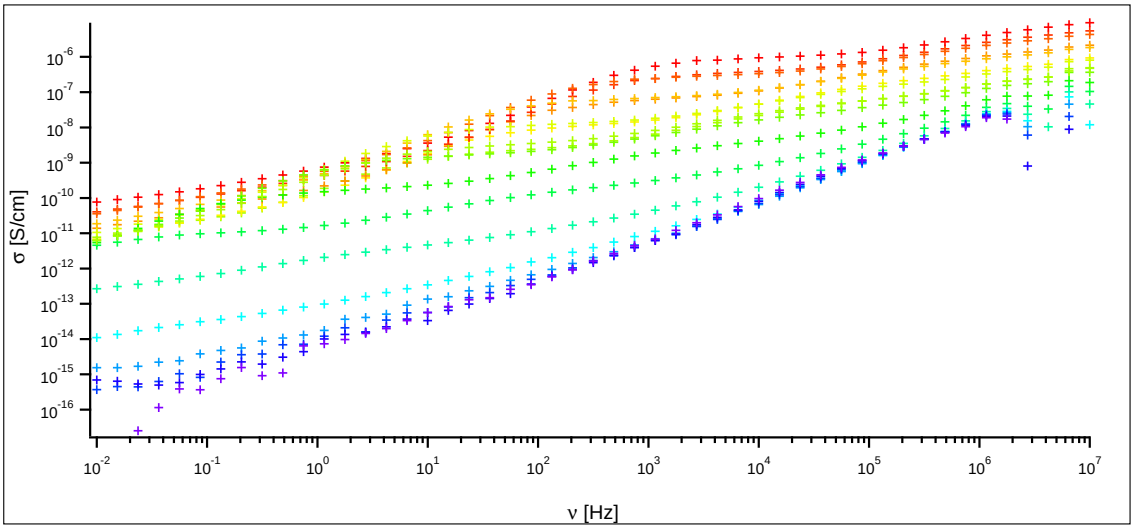

Figure A.32: Impedance results for the PEO membrane with 10 wt% MIL-53NH_2(Al)

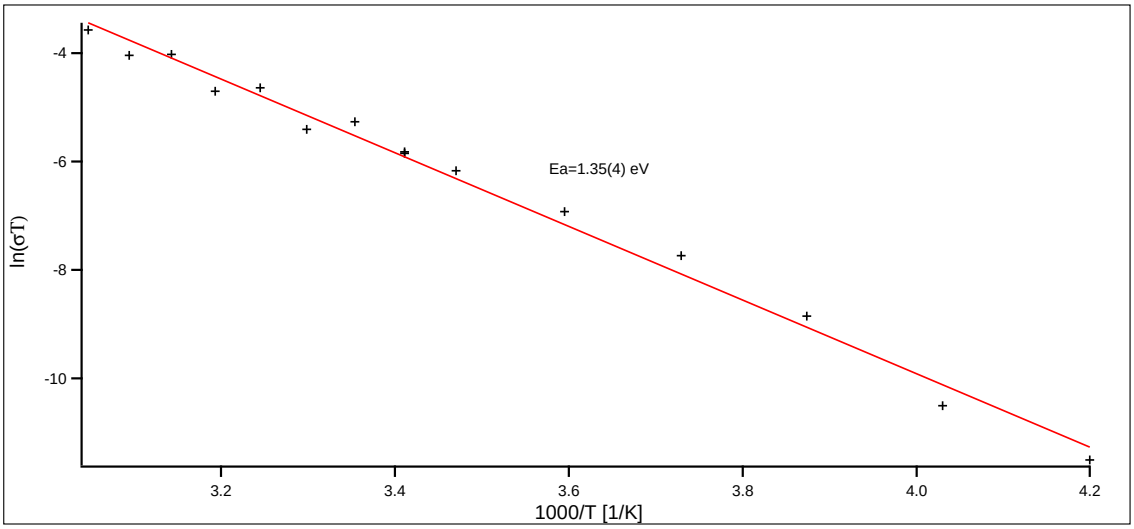

Figure A.33: Arrhenius plot for the PEO membrane with 10 wt% MIL-53NH_2(Al)